Bi_2WO_6-based Z-scheme photocatalysts: Principles, mechanisms and photocatalytic applications

Tamer M. Khedr[1,2,*], Kunlei Wang[1,3], Damian Kowalski[4], Said M. El-Sheikh[2], Hany M. Abdeldayem[5], Bunsho Ohtani[1] and Ewa Kowalska[1,*]

[1]Institute for Catalysis, Hokkaido University, N21, W10, Sapporo 001-0021, Japan
[2]Nanomaterials and Nanotechnology Department, Advanced Materials Institute, Central Metallurgical Research and Development Institute (CMRDI) P.O. Box: 87 Helwan, Cairo 11421, Egypt
[3]Northwest Research Institute, Co. Ltd. of C.R.E.C., 730000, Lanzhou, P.R. China
[4]Faculty of Chemistry and Biological and Chemical Research Centre, University of Warsaw, Zwirki i Wigury 101, 02-089 Warsaw, Poland
[5]Chemistry Department, Faculty of Science, Ain Shams University, 11566 Abassia, Cairo, Egypt

* Correspondence: tamerkhedr56@gmail.com (T.M.K.) and kowalska@cat.hokudai.ac.jp (E.K.)

Abstract: The development of novel photocatalysts for efficient utilization of solar energy is highly essential for the most critical humanitarian challenges, i.e., energy and water crises as well as environmental pollution. Bismuth tungstate (Bi_2WO_6), an outstanding Aurivillius phase perovskite, has attracted intensive attention as a visible-light-responsive photocatalyst because of its non-toxicity, low cost, and outstanding physicochemical characteristics, i.e., nonlinear dielectric susceptibility, ferroelectric piezoelectricity, pyroelectricity, catalytic behavior, modifiable morphology, strong oxidation power, and good photochemical stability. However, the photocatalytic activity of bare Bi_2WO_6 is restricted because of the inherent drawbacks such as poor light-harvesting efficiency, weak reduction potential, relatively low specific surface area, the fast recombination rate of photoinduced charge carriers, and thus poor quantum yields of photocatalytic reactions. Moreover, the impossibility of simultaneous strong redox ability (demanding wide bandgap) and high light-harvesting efficiency (requiring narrow bandgap) is considered as a big challenge for the practical application of Bi_2WO_6. Undeniably, the construction of Z-scheme photocatalytic systems is recommended strategy to overcome the above-mentioned disadvantages because of the efficient spatial separation of photogenerated charge carriers and the boosting the redox performance. This review summarizes the principles and recent developments on Z-scheme photocatalytic systems with special emphasis on the Bi_2WO_6-based photocatalysts, including the types, photocatalytic mechanisms and practical applications. Moreover, major differences between type-II heterojunction and Z-scheme photocatalyst have also been discussed. Additionally, the significant role of unique structures (e.g., core-shell and 2D/2D) for the improvement of photocatalytic activity of Z-scheme photocatalyst has been presented. Indeed, Bi_2WO_6-based Z-scheme photocatalysts have exhibited superior photocatalytic activity for various applications. For example, they show high photocatalytic activity towards water/wastewater treatment (removal of organic and inorganic pollutants, as well as microorganisms), air purification (decomposition of volatile organic compounds and inorganic matters), “green” energy conversion (e.g., generation of H_2 and CH_4 fuels under solar irradiation), and organic synthesis. It is thought that this remarkable activity of Bi_2WO_6-based Z-scheme photocatalysts might be attributed to the efficient solar light harvesting, separation and further transfer of charge carriers and strong redox ability. To the best of our knowledge, the present paper is the first attempt to summarize the Bi_2WO_6-based Z-scheme photocatalytic reactions, providing important insights and up-to-date information for the scientific community to fully explore the potential of Bi_2WO_6-based photocatalysts for renewable environmental remediation, energy conversion, and chemical synthesis.

Keywords: Bi_2WO_6; Z-scheme photocatalyst; environmental purification, energy conversion; organic synthesis; green energy; solar photocatalysis, coupled semiconductors

1. Introduction

Fast-growing environmental pollution and the global energy crisis are probably the most serious threats to human life and property. Therefore, various methods of environmental purification and energy generation have been intensively examined in recent times. For example, advanced oxidation processes (AOPs), also known as advanced oxidation technologies (AOTs), have been proposed as efficient methods, especially for environmental treatment, since reactive oxygen species (ROS, mainly hydroxyl radicals), formed in-situ, are highly active against organic and inorganic compounds, as well as microorganisms. Usually, ROS, e.g., hydroxyl radical ($^{\bullet}OH$), superoxide radical ($^{\bullet -}O_2$), sulfate radical ($SO_4^{\bullet -}$), ferrate radical (FeO_4^{2-}) and ozone (O_3), are generated using primary oxidants, e.g., hydrogen peroxide (H_2O_2), persulfate, ferrate, permanganate, and oxygen or via physical methods. Unfortunately, majority of these methods, e.g., supercritical water oxidation (SCWO), wet air oxidation (WAO) and UV-based irradiation systems (UV/O_3 and UV/H_2O_2), require high energy demands, continuous feeding of reagents (e.g., H_2O_2, O_3) and high investment and operating costs. It has been thought that heterogeneous photocatalysis is probably the best AOP method, as solar energy might be used for photocatalyst excitation even for wide-bandgap semiconductors (e.g., TiO_2 and ZnO). Accordingly, various reports have been published on the synthesis, property-governed activities, mechanism clarifications, activity improvements and possible applications of heterogeneous photocatalysis, especially for TiO_2 photocatalysts (the most broadly investigated photocatalyst) [1-4]. However, titania must be excited with UV irradiation, and thus only slight part of solar radiation (ca. 2%) might be efficiently used for photocatalytic reactions. Therefore, various methods of wide-bandgap semiconductors' modification have been proposed, including doping, surface modification and formation of composite photocatalysts. It is thought that the last-listed above, i.e., composite photocatalysts, might be the most attractive since both inhibition of charge carriers' recombination and appearance of vis activity might be achieved by proper selection of constituent parts. It should be pointed out that not only the modification of well-known materials, but also preparation of novel photocatalysts with vis response has been intensively studied, e.g., graphitic carbon nitride (g-C_3N_4), WO_3, CuO, Cu_2O, $SrTiO_3$, $BiVO_4$, Ta_3N_5, TaON, $CaTaO_2N$, $SrTaO_2N$, $BaTaO_2N$ (e.g., [5-9]).

First, the basic mechanism of heterogeneous photocatalysis should be presented. Three sequential and integral steps are as follows: 1) photocatalyst (semiconductor) activation under irradiation with energy equal or larger than its energy gap (E_g), resulting in charge carriers' generation, i.e., electrons in the conduction band (CB) and holes in the valence band (VB), 2) charge carriers' transfer, i.e., migration to the photocatalyst surface or recombination (bulk/surface), 3) surface redox reactions (Fig. S1). It should be pointed out that the photocatalysis thermodynamics, which is governed by the band levels (CB and VB) and redox potentials of adsorbed reactants (acceptor and donor), and the photocatalysis kinetics (i.e., charge generation, migration and consumption), are highly critical for the photocatalytic efficiency [10,11]. Thermodynamically, the redox potential of oxidant (acceptor) should be below (more positive than) the conduction band minimum (CBM) of the semiconductor to proceed the reduction reactions, whereas the redox potential of the reductant (donor) should be more negative than the valence band maximum (VBM) to attain the oxidation reactions. Therefore, for superior photocatalytic activity, the semiconductor needs to have strong redox ability, which demands a wide bandgap (from the thermodynamic viewpoint) and wide light-harvesting range, which requires a narrow bandgap (from the kinetic viewpoint). Obviously, the balance between thermodynamics and kinetics to attain high-performance photocatalysts is impossible to be achieved in traditional (i.e., single component) photocatalyst. Therefore, the multi-component (heterojunctions) photocatalysts, composed of two or more semiconductors with different oxidation and redox potentials, have been proposed for efficient light harvesting and high quantum efficiencies.

Three types of heterojunction between two semiconductors could be distinguished, i.e., i) type-I ("straddling gap", Fig. 1a, e.g., α-Fe_2O_3/TiO_2), ii) type-II ("staggered gap", Fig. 1b, e.g., Cu_2O/TiO_2), and iii) type-III ("broken gap", Fig. 1c). Obviously, the type-II heterojunction is the most recommended for photocatalytic applications, because of the spatial separation of charge carriers (an opposite direction of electron and hole transfer), resulting in inhibition of charge carriers' recombination, and thus an increase in the photocatalytic efficiency. Typically, the type-II heterojunction photocatalysts contain two semiconductors (SCI and SCII) with staggered band structure configuration, as shown in Fig. 1b. Under irradiation (with an energy equal or larger than their band gaps), both SCI and SCII are simultaneously excited, and thus formed charge carriers (electrons in CB and holes in VB) might migrate between semiconductors, i.e., electrons from SCI (of more negative CB) to SCII (of less negative CB), and holes from SCII (of more positive VB) to SCI (of less positive VB), resulting in accumulation of electrons and holes in SCII and SCI, respectively. Although, the separation of charge carriers in type-II heterojunction results in inhibition of charge carriers' recombination, the redox ability (the thermodynamic viewpoint), is lower than that in singlet-component photocatalysts since the holes and electrons are accumulated at the lower and higher potential of VB and CB (i.e., less positive and less negative), respectively. Additionally, the electrostatic repulsions between symmetrically charged components restrict the charge carriers' migration between two semiconductors (the kinetic viewpoint).

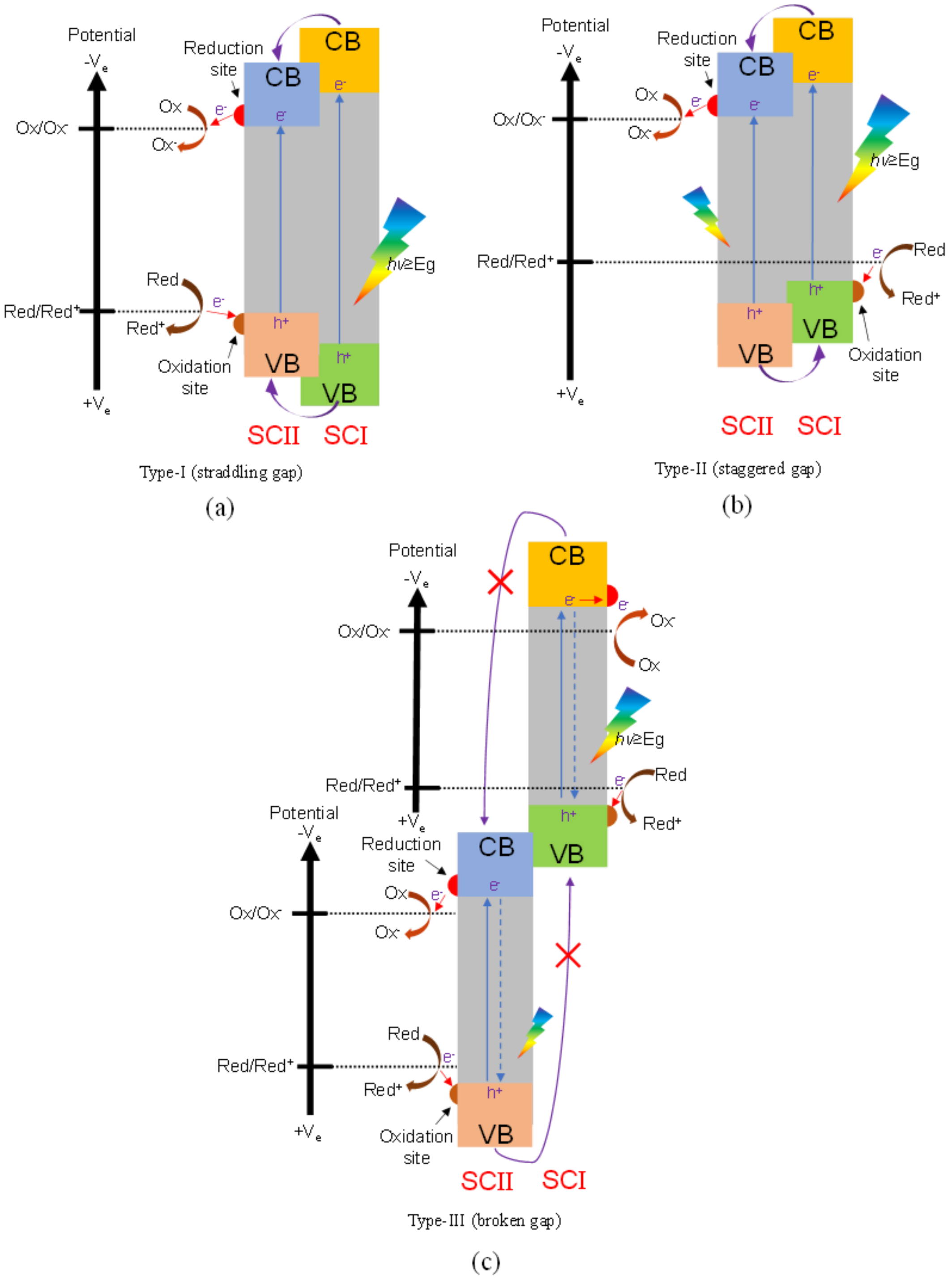

Fig. 1. The schematic drawings for semiconductor-based heterojunctions: type I **(a)**, type II **(b)** and type III **(c)**. Ox: oxidant, Red: reductant.

Based on these aspects, a dilemma on the efficient heterojunctions has been raised, i.e., how to prepare efficient and stable heterojunction photocatalysts with efficient separation of charge carriers and strong redox ability. Therefore, it has been proposed that the new system must be designed to overcome these limitations. Accordingly, the nature has inspired scientists as the photosynthesis occurring in the green plants might be adapted for the photocatalytic reactions by the construction of the artificial photosynthesis systems, named as Z-scheme heterojunctions [5,12-14]. The Z-scheme mechanism occurs naturally in green plants through photosynthesis process ("natural Z-scheme photocatalysis"), in which the charges migration route shows a two-step photoexcitation, which looks like the letter "Z" turned 90^{o} counterclockwise ("the zigzag"), as shortly presented in SI (Fig. S2).

The artificial Z-scheme photocatalytic system (ZSPS) is generally composed of two semiconductors (SCI & SCII) and charge mediator, classified into three groups, as follows. (1) Liquid-phase Z-scheme/traditional Z-scheme (1^{st}-generation Z-scheme, Fig. 2a), which contains an aqueous redox-pair mediator, i.e., shuttle redox mediator, including $Fe^{3+/2+}$, IO_3^{-}/I^{-} and $[Fe(CN)_6]^{3-/4-}$. (2) All-solid-state Z-scheme (2^{nd}-generation Z-scheme, Fig. 2b), which consists of a solid mediator, such as metals (Ag, Pt, Au), reduced graphene oxide (RGO) and carbon nanotubes (CNTs). (3) Direct Z-scheme (3^{rd} generation Z-scheme, Fig. 2c), which does not contain any charge mediator. Upon irradiation, electron/hole pairs are generated in the CB/VB of both semiconductors. Then, the photogenerated low-energy electrons (at the CB of SCII) recombine with low-energy holes (at the VB of SCI) directly (direct Z-scheme) or with the help of redox-mediator, whereas the high-energy electrons (strong reducer) and holes (strong oxidizer) in the CB of SCI and the VB of SCII, respectively, react with adsorbed compounds via respective redox reactions (Table S1). As mentioned above, the Z-scheme photocatalysts outperform the type-II heterojunction due to strong redox ability, since the photogenerated electrons and holes are more negative and more positive, respectively, and they are spatially separated.

It should be pointed out that Z-scheme photocatalytic systems might be constructed from semiconductors with visible-light (vis) absorption (narrower bandgap than that in titania), and thus efficient light harvesting at broad solar radiation range could be achieved.

Accordingly, visible-light-responsive (VLR) bismuth-based photocatalysts, such as Bi_2O_3, BiOX (X = Br, I), $BiVO_4$, Bi_2MoO_6, Bi_2WO_6, have attracted great attention because of their significant photocatalytic activity for environmental decontamination as well as oxygen evolution during water splitting [15,16]. For example, bismuth tungstate (Bi_2WO_6, n-type semiconductor) has recently been considered as a promising material, especially for photocatalytic oxidation reactions, because of its excellent intrinsic physicochemical characteristics, such as optical/electronic properties, including VLR (bandgap of ca. 2.8 eV), nonlinear dielectric susceptibility, ferroelectric piezoelectricity, pyroelectricity, strong oxidation potential, catalytic behavior, photostability, low cost, and non-toxicity [17-19]. However, the practical application of Bi_2WO_6 (BWO) is limited by the rapid electron-hole recombination (low efficiency of charge carriers' separation) and low photo-harvesting ability. As a class of highlighted strategies, the construction of BWO-based Z-scheme photocatalytic systems with an effective spatial separation of charge carriers as well as strong redox properties and high light harvesting efficiency, has attracted substantial research interest for efficient solar-energy conversion (i.e., as broad "green" applications).

Accordingly, this review presents the development of BWO-based photocatalysts, including their types, preparation, characterization, mechanism clarifications and various applications, including environmental purification, solar-fuel generation and synthesis of organic compounds.

Although, it is of importance to follow the historical development of Z-scheme photocatalytic systems (from the first-generation to the third-generation ones) to understand the principles, mechanisms, nano-architecture design, advantageous and shortcomings of various materials, due to journal policy ("to keep the review manuscripts concise and readable") this part has been placed in SI (including Fig. S3-S7).

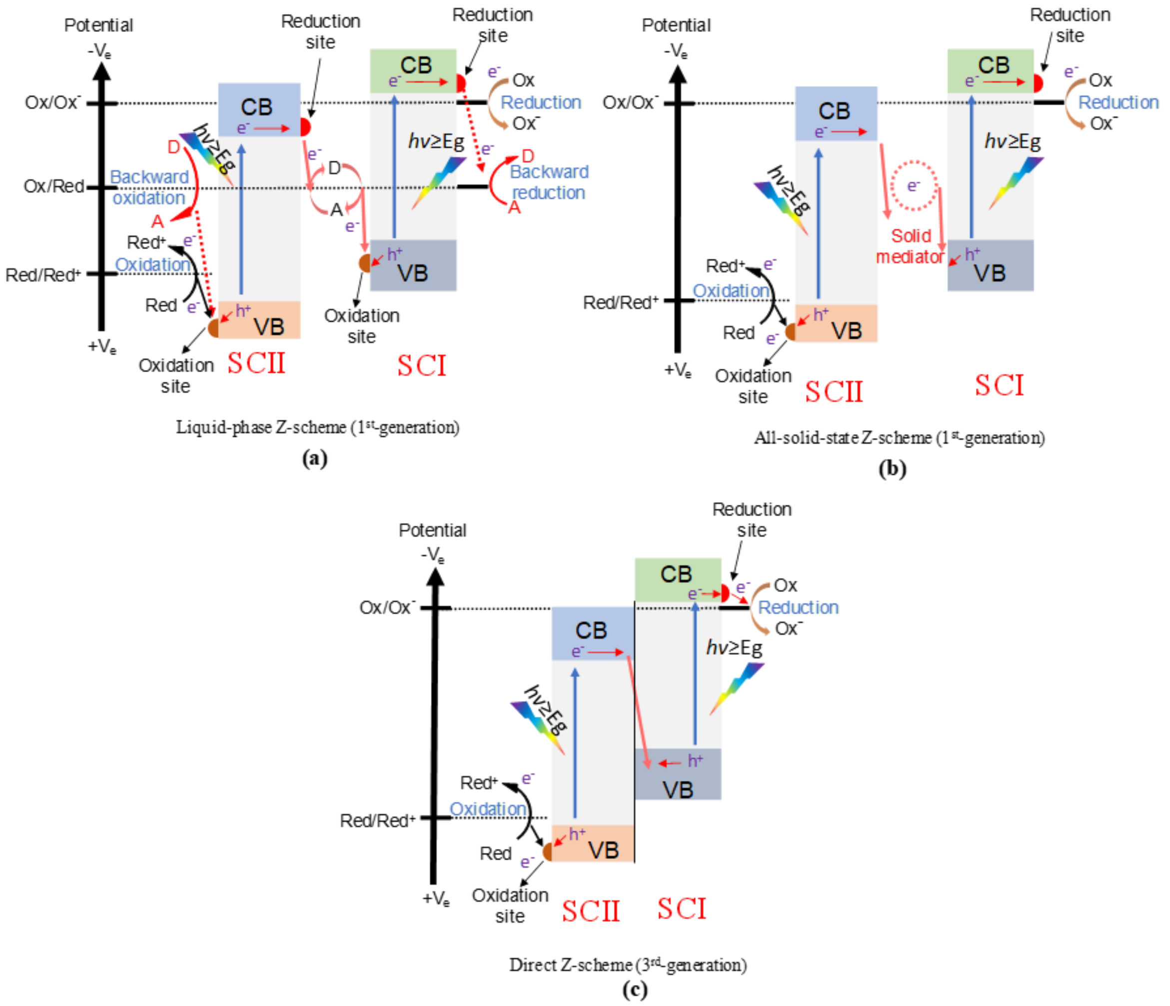

Fig. 2. The schematic drawings showing artificial Z-scheme photocatalytic systems: liquid-phase Z-scheme **(a)**, all-solid-state Z-scheme **(b)** and direct Z-scheme **(c)**. A: acceptor, D: donor, Ox: oxidant, Red: reductant.

2. Bi_2WO_6-based Z-scheme photocatalysts

Bismuth tungstate (Bi_2WO_6; BWO) has been considered as a novel and promising VLR photocatalyst for photooxidation of organic pollutants because of its unique structure (a perovskite-type layered), superb physicochemical characteristics, chemical stability, non-toxicity, low cost, strong oxidation power, and vis harvesting ability (band gap of ca. 2.8 eV) [17-19]. BWO can be found in nature as mineral russellite, named in honor of Sir Arthur Edward Ian Montagu Russell (1878-1964), British mineral collector (arthurite mineral was also named in his and Arthur W. G. Kingsbury honor). Russellite is an orthorhombic –

pyramidal mineral of various tints (brown-orange, greenish, greenish yellow and light yellow) and ferroelectric properties [20]. Russellite is the simplest member of the Aurivillius phase compounds, i.e., a form of perovskite with the general formula of $Me_2O_2(Me'_{n-1}R_nO_{3n+1})$, where Me is a large 12 co-ordinate cation (here Bi), and R is a small 6 co-ordinate cation (here W). The structure of russellite is built up of $Bi_2O_2^{2+}$ slabs between WO_4^{2-} layers.

The Aurivillius phases are the compounds having $(Bi_2O_2)(A_{n-1}B_nO_{3n+1})$ structure, composed of alternating layers of $(Bi_2O_2)^{2+}$ and perovskite-like blocs. One of this type of structures having A site absent in the oxide with a general formula of $(Bi_2O_2)(BO_4)$ is bismuth tungstate Bi_2WO_6. For bismuth tungstate, the WO_6 units construct two-dimensional network of corner-sharing octahedra, which is one WO_6 layer thick. At ambient temperature the Bi_2WO_6 crystallizes in orthorhombic crystal system with 29 $P2_1ab$ symmetry [21,22]. The transition from the space group 29 $P2_1ab$ to higher symmetry 41 B2cb has been suggested to occur at approximately 660 ^oC [23], whereas the earlier studies reported high symmetry at lower temperatures [24]. This transition corresponds to the loss of one octahedral tilt mode in the pseudo-perovskite layer [23,25]. The additional phase transition occurs at 960 ^oC, which corresponds to ferroelectric Curie point. The phase structure formed at $T > 960$ ^oC is under debate; according to Watanabe the structure might be similar to $BiLaWO_6$, in which the Bi_2O_2 layers essentially remain unchanged, whereas pseudo-perovskite blocks, constructed at the corner-sharing WO_6 octahedra, are reconstructed to WO_4 tetrahedra [26]. In contrast to this observation, McDowell et al. have found that high temperature phase is composed of alternating Bi_2O_2 layers and perovskite-like layers reconstructed from corner-sharing into edge-sharing WO_6 octahedra [23,27]. The medium temperature phase of Bi_2WO_6 having 41

B2cb symmetry is shown in Fig. 3. The unit cell has lattice parameters of a = 5.5340 Å, b = 5.4998 Å, c = 16.5507 Å and cell volume of 503.7381 $Å^3$.

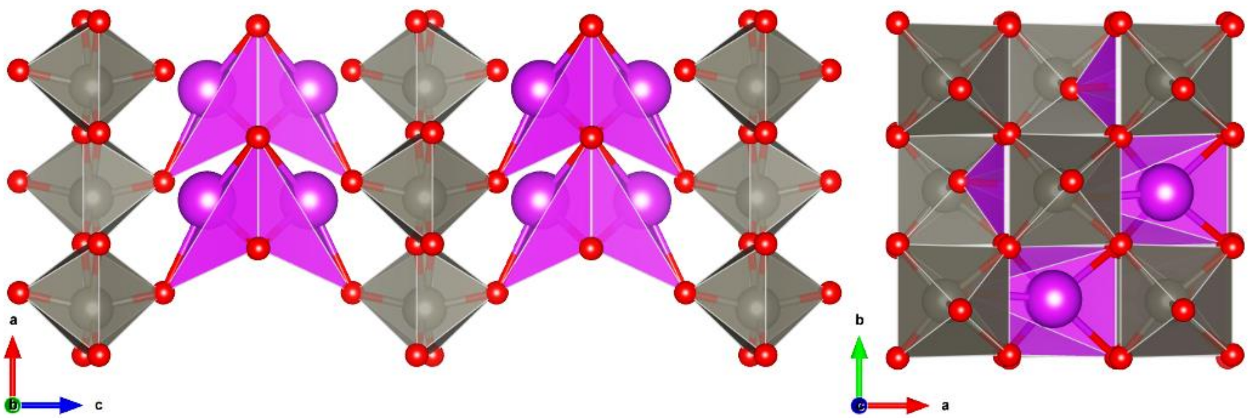

Fig. 3. Structure of Bi_2WO_6 displaying the WO_4^{2-} and $Bi_2O_2^{2+}$ layers.

BWO has already been proposed for various applications, including: i) piezoelectric devices as a lead-free material, because of high ferroelectric Curie point (Tc ≃ 960 °C) and high electromechanical coupling coefficient, ii) an electrode material for solid oxide fuel cells due to its high oxide ion conductivity, iii) medical applications (tumor radiosensitization, and photothermal/photodynamic therapy of cancer), iv) catalyst, e.g., oxidation of methane to methanol, and v) photocatalyst, as discussed further in this paper [28-30].

For example, Lai et al. prepared nanospherical Bi_2WO_6 by solvothermal method for photocatalytic degradation of Erichrome Black T dye under solar radiation [30]. However, the rapid recombination of the photogenerated charge carriers, low reduction ability and limited light-harvesting efficiency have resulted in low interest for the practical applications of a one-component BWO for photocatalysis [17-19]. Accordingly, increasing efforts have been made to overcome these shortcomings, e.g., by construction of BWO-based Z-scheme photocatalysts, including mediated-Z-scheme (all-solid-state Z-scheme) using different solid mediators, such as Ag [31-34], Au [35,36], Pt [37,38], Bi [39–42], Cu [43], Zn [44], oxygen vacancies (OV) [45], polypyrrole (PPy) [46], RGO [47-51], CNT [52-54], and Mxenes (Ti_3C_2) [55], and mediator-free Z-scheme (direct Z-scheme) [56–68] (Fig. 2a).

For instance, novel Z-scheme In_2S_3/Bi_2WO_6 core-shell photocatalyst was controllably fabricated for the improvement of photocatalytic degradation of tetracycline hydrochloride (TC) antibiotic under vis irradiation (500-W Xe lamp with a UV cut-off filter, $\lambda > 420$ nm) [69]. First, the pristine In_2S_3 micro/nanospheres were synthesized by hydrothermal method, followed by self-etching. Then, the binary In_2S_3/Bi_2WO_6 photocatalyst was prepared via template/hydrothermal method with different compositions (In_2S_3: 0–40 wt%). The photocatalytic activity of these photocatalysts (In_2S_3, Bi_2WO_6, and In_2S_3/Bi_2WO_6 composites: 20%In_2S_3/Bi_2WO_6, 30%In_2S_3/Bi_2WO_6 and 40%In_2S_3/Bi_2WO_6) are shown in Fig. 4a. Although the photocatalytic activity of bare samples (In_2S_3 and Bi_2WO_6) is not high (only 40.0% and 45.0% degradation rate, respectively), probably due to the rapid recombination of photoinduced charge carriers, the 30%In_2S_3/Bi_2WO_6 composite shows 2.4- and 2.1-fold higher activity, respectively, and high stability (Fig. 4b). It has been proposed that the activity improvement has been caused by the core-shell morphology, polycrystalline structure, enhanced light absorption efficiency, effective charge carriers' transfer and separation through Z-scheme mechanism. The interface in core-shell structure might ensure an interfacial transfer of charges, i.e., from the VB of In_2S_3 to the CB of Bi_2WO_6, generating the built-in electric field, and thus facilitating the migration of charge carriers in accordance with Z-scheme mechanism, as shown in Fig. 4c. Moreover, the core-shell structure (Bi_2WO_6 shells on the In_2S_3 core) could provide more reactive sites, hence boosting the photocatalytic performance.

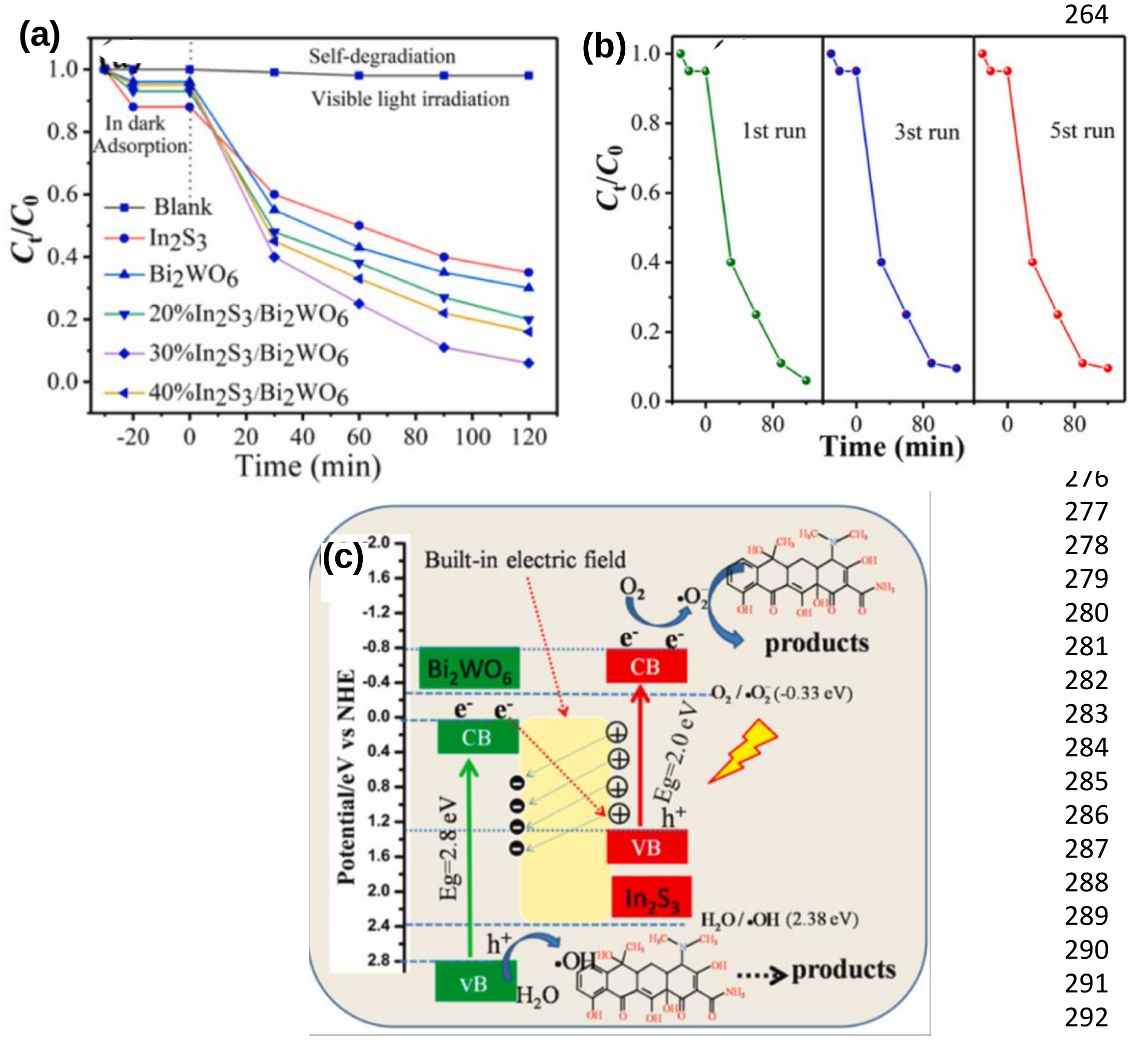

Fig. 4. **(a)** Photocatalytic activity (tetracycline hydrochloride antibiotic degradation during 2-h vis irradiation) data of Bi_2WO_6, In_2S_3, and In_2S_3/Bi_2WO_6 composites prepared for different contents of In_2S_3 (20-40 wt.%), **(b)** stability data for fresh and recycled sample (30 wt%In_2S_3/Bi_2WO_6), and **(c)** schematic drawing showing Z-scheme mechanism for In_2S_3/Bi_2WO_6 composite under vis irradiation. Reproduced from Ref. [69], copyright 2022, with permission from Elsevier.

2.1. Methods used for Z-scheme mechanism elucidation of Bi_2WO_6-based photocatalysts

Various methods have been proposed for the clarification of the mechanism (mainly charge carriers' transfer) of Bi_2WO_6-based Z-scheme photocatalysts, including experimental methods, such as, reactive species trapping (using different scavengers), 5,5-dimethyl-pyrroline N-oxide (DMPO)-ESR analysis, terepthalic acid-photoluminescence (TA-PL), photocatalytic reduction tests, in-situ X-ray photoelectron spectroscopy (XPS), and band structure characterizations as well as corresponding theoretical analysis (Mott-Schottky analysis and density functional theory (DFT) calculations), as shortly presented in the following subsections. It should be pointed out that using only one method might not give accurate elucidating for the charge carriers' transfer mechanism in the Z-scheme photocatalytic system. Therefore, the combination of different approaches is required to prove the construction of Z-scheme.

2.1.1. Experimental methods

It is well known that photocatalytic oxidation reactions (oxidative decomposition of organic compounds and microorganisms, and O_2 generation) on the surface of photocatalyst by photogenerated charge carriers (e^- and h^+) can only proceed when there is sufficient potential to produce reactive oxygen species (ROS), including $^{\bullet}OH$ (standard redox potential of $^{\bullet}OH/H_2O$ of 2.4 V *vs.* NHE) and $^{\bullet}O_2^-$ (standard redox potential of $O_2/^{\bullet}O_2^-$ of −0.33 V *vs.* NHE) radicals [70,71]. Therefore, the mechanism of the Bi_2WO_6-based Z-scheme photocatalytic systems could be elucidated by detecting these ROS generated during photocatalytic reactions. Commonly, ROS could be estimated by following experiments: (i) trapping tests, in which different scavengers are used to capture h^+, $^{\bullet}OH$ and $^{\bullet}O_2^-$, (ii) electron spin-resonance (ESR) analysis (5,5-dimethyl-pyrroline N-oxide, DMPO, is used to probe $^{\bullet}OH$ and $^{\bullet}O_2^-$, producing DMPO−$^{\bullet}OH$ and DMPO−$^{\bullet}O_2^-$, respectively), and (iii) photoluminescence (PL) experiments in the presence of nonflourescent terepthalic acid (TA), which reacts with $^{\bullet}OH$, resulting in formation of highly fluorescent 2-hydroxyterephathalic acid (HTA).

For instance, the photocatalytic degradation of antibiotic tetracycline over the binary $Bi_2WO_6/CuBi_2O_4$ nanocomposite was examined in the absence and the presence of various scavengers, such as disodium ethylenediamine tetraacetic acid (EDTA), tert-butanol (t-BuOH), and 1,4-benzoquinone (BQ) to capture h^+, $^{\bullet}OH$ and $^{\bullet}O_2^-$, respectively, and also N_2 purging was performed to confirm the importance of O_2 during reaction, and obtained data are shown in Fig. 5a [72]. Obviously, the photocatalytic activity was significantly decreased from 86% to 57%, 56% and 54% after addition of BQ and EDTA, and by N_2 purging, respectively. However, there was only slight change after t-BuOH addition, indicating that $^{\bullet}O_2^{-}$, h^+ and O_2 were crucial for tetracycline degradation, whereas $^{\bullet}OH$ radicals had a minor role. These results were further investigated by ESR analysis, as shown in Fig. 5 (b and c). It was found that pristine Bi_2WO_6 was inactive for production of $^{\bullet}O_2^{-}$ (Fig. 5b), whereas significant $^{\bullet}OH$ signals were observed for $Bi_2WO_6/CuBi_2O_4$ composite (Fig. 5c). These results have indicated that the photogenerated electrons and holes in the $Bi_2WO_6/CuBi_2O_4$ composite photocatalyst are able to form $^{\bullet}O_2^{-}$ and $^{\bullet}OH$, whereas the potential of photogenerated electrons in Bi_2WO_6 is not sufficient to produce $^{\bullet}O_2^{-}$. It is not surprising after consideration that CB and VB levels of Bi_2WO_6 and $CuBi_2O_4$ are 0.33 V and -0.42 V, and 3.11 V and 1.37 V (*vs.* NHE), respectively. Therefore, only photogenerated electrons in $CuBi_2O_4$ could reduce O_2 to produce $^{\bullet}O_2^{-}$ (E ($O_2/^{\bullet}O_2^{-}$) = -0.33 V *vs.* NHE), and similarly only photogenerated holes in Bi_2WO_6 could oxidize H_2O to generate $^{\bullet}OH$ (E ($H_2O/^{\bullet}OH$) = 2.4 V *vs.* NHE), as shown in Fig. 5d. These results demonstrate that the electrons could not migrate from CB of $CuBi_2O_4$ to CB of Bi_2WO_6 via type-II heterojunction, but rather the Z-scheme mechanism should be considered (Fig. 5d).

The $^{\bullet}OH$ radicals were also detected by PL of HTA ($\lambda_{exc.}$ = 315 nm) for C-dots@TiO_2/Bi_2WO_6 composite photocatalyst, as shown in Fig. 6a [73]. It was found that PL intensity of HTA increased with an increase in the irradiation time, indicating that the photocatalyst possessed adequate oxidation potential to generate $^{\bullet}OH$ radicals (conversion of TA into HTA). Considering that the CB and VB potentials of Bi_2WO_6 are 0.595 V and 3.2 V, respectively, and -0.21 V and 2.8 V are respective values for TiO_2, it has been suggested that only photogenerated holes at the VB of Bi_2WO_6 could produce $^{\bullet}OH$, whereas O_2 could be only reduced into $^{\bullet}O_2^{-}$ on the CB of TiO_2 (Fig. 6b), and thus Z-scheme mechanism was also suggested in this system. Although Z-scheme mechanism is highly recommended for high activity, and obtained data could indirectly confirm it, it should be remembered that TiO_2 is known to be effective to form hydroxyl radicals (slight differences in VB bottom have been reported). Moreover, the generation of hydroxyl radical by both redox pathways should be also considered, i.e., via photogenerated holes (as discussed here), but also due to further reaction of $^{\bullet}O_2^-$ radicals (formed from adsorbed oxygen and photogenerated electrons) with water (via H_2O_2).

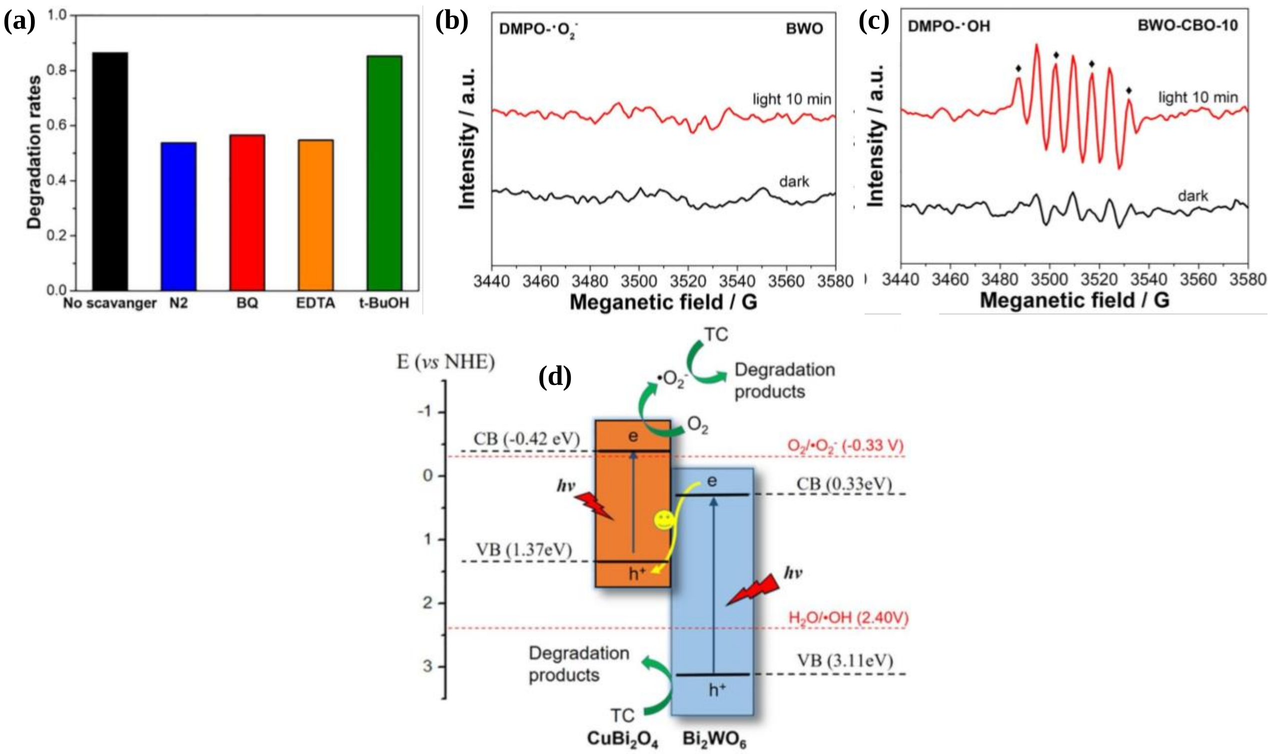

Fig. 5. (a) The photodegradation activity of tetracycline (15 mg L^{-1}) over $Bi_2WO_6/CuBi_2O_4$ photocatalyst in the presence of different scavengers (BQ, EDTA and t-BuOH) or N_2 purging, **(b-c)** DMPO spin-trapping ESR spectra of: **(b)** Bi_2WO_6 in methanol dispersion for DMPO–$^{\bullet}O_2^-$ and **(c)** $Bi_2WO_6/CuBi_2O_4$ in aqueous dispersion for DMPO–$^{\bullet}$OH, and **(d)** the schematic drawing showing the Z-scheme mechanism of tetracycline degradation on $Bi_2WO_6/CuBi_2O_4$. Reproduced from Ref. [72], copyright 2019, with permission from Elsevier.

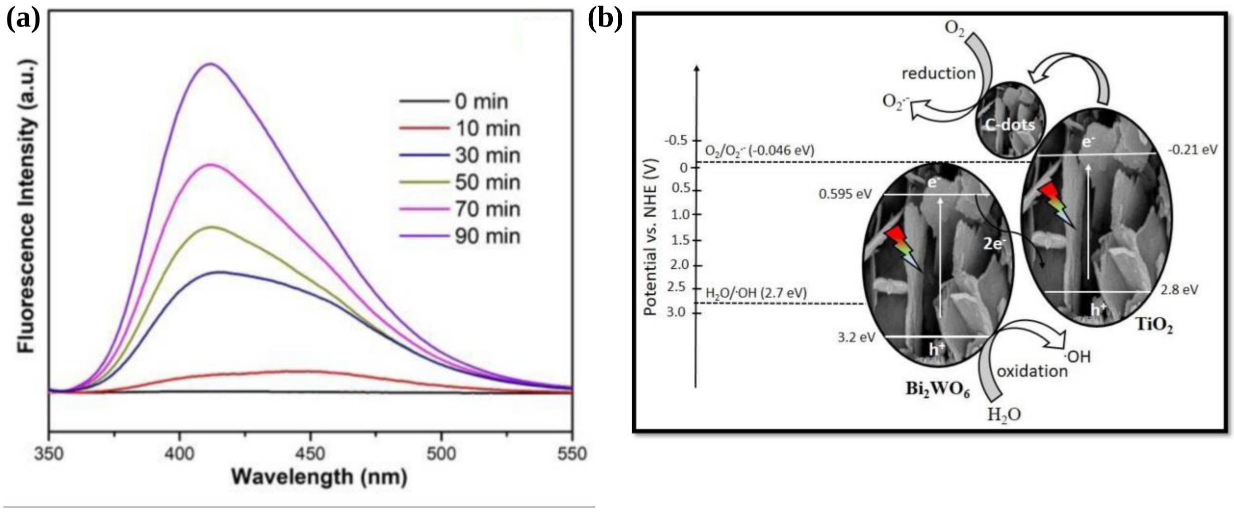

Fig. 6. (a) PL spectra of the C-dots@TiO_2/Bi_2WO_6 photocatalyst under different duration of solar radiation in a basic solution of terephthalic acid, and **(b)** the proposed mechanism of levofloxacin degradation on the direct C-dots@TiO_2/Bi_2WO_6 Z-scheme photocatalyst [73].

In contrast to photocatalytic oxidation reactions, photocatalytic reduction reactions (e.g., reduction of organic and inorganic compounds, H_2 generation, CO_2 reduction and organic synthesis) involve the reactions on the surface of the photocatalysts by the photogenerated electrons with a suitable potential for specific reaction, and thus photogenerated holes are usually scavenged during these experiments, e.g., by alcohol addition. Accordingly, the Z-scheme formation could be confirmed by detecting the accumulation of the photogenerated electrons on a specific semiconductor of the Z-scheme photocatalytic system during photoreduction. For example, it was suggested that during overall water splitting over the binary Bi_2WO_6/Cu_3P composite under solar light irradiation only Cu_3P could cause water reduction, considering the CB and VB levels of Bi_2WO_6 (0.22 V and 3.02 V, respectively) and Cu_3P (-0.64 V and 1.02 V, respectively) [74]. These results have suggested that in the case of Bi_2WO_6/Cu_3P photocatalyst, the heterojunction (type-II) (Fig. 7a) could only result in water oxidation, whereas the overall water splitting might be only achieved via Z-scheme mechanism (Fig. 7b).

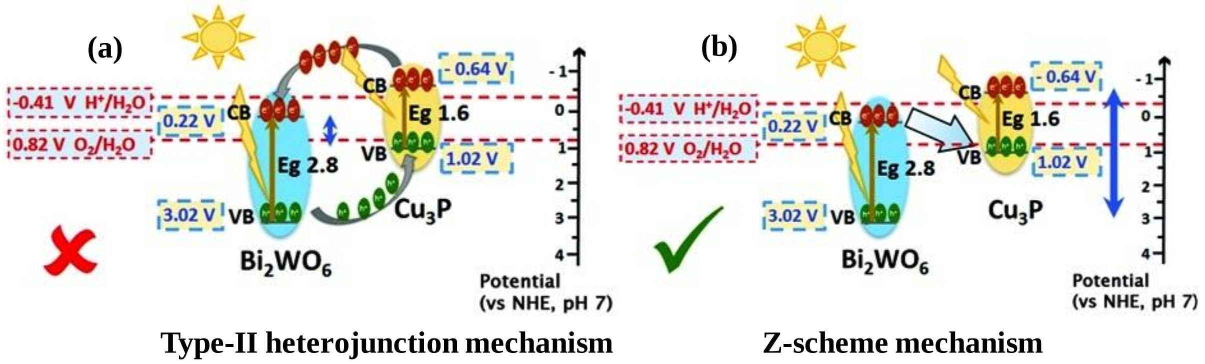

Fig. 7. The schematic drawings of charge carriers' transfer for Bi_2WO_6/Cu_3P photocatalyst in the case of: **(a)** type-II heterojunction and **(b)** Z-scheme photocatalyst. Reproduced from Ref. [74], copyright 2018, with permission from RSC.

X-ray photoelectron spectroscopy (XPS) analysis is usually used to investigate the surface properties of materials, such as chemical composition and oxidation states of elements. Recently, XPS analysis has also been applied to confirm the formation of Z-scheme photocatalytic systemes via evaluation of the shift in binding energies, i.e., positive/negative through losing/receiving electrons, respectively, as well as the changes in the oxidation states of elements after irradiation. Accordingly, after the formation of Z-scheme photocatalytic system between two semiconductors with different electronic properties, the electrons are transfered from the semiconductor of higher Fermi level to that with lower one till two Fermi levels are aligned to the same level, resulting in the change of binding energy of the specific elements. Furthermore, when the Z-scheme photocatalyst is photoexcited, photogenerated charge carriers' migration takes place at the interface between two semiconductors, which might also result in the change of oxidation state of elements (in the case of incomplete charge carriers' consumption). Therefore, XPS could be also used to investigate the pathway of charge transfer in the Bi_2WO_6-based Z-scheme photocatalytic systems. For example, Yuan et al. have confirmed the formation of $Bi_2WO_6/CuBi_2O_4$ Z-scheme by the shift towards the higher binding energy for Cu2p (Fig. 8a), Bi4f (Fig. 8b) and O1s (Fig. 8c) in comparison with the pristine $CuBi_2O_4$ photocatalyst [72]. It was found that the binding energy of Cu2p in the pure $CuBi_2O_4$ could be assigned to Cu^{2+}, whereas, that in the $Bi_2WO_6/CuBi_2O_4$ composite could be attributed to Cu^{+}. It has been proposed that the electrons are transferred from $CuBi_2O_4$ to Bi_2WO_6 after heterojunction formation for creating an electric field between $CuBi_2O_4$ to Bi_2WO_6. During XPS analysis, both semiconductors are photoexcited, and hence the photogenerated electrons might migrate from Bi_2WO_6 to $CuBi_2O_4$ under the effect of internal electric field. Accordingly, the formation of $Bi_2WO_6/CuBi_2O_4$ Z-scheme has been confirmed by XPS analysis and trapping tests, as discussed above (Fig. 5d).

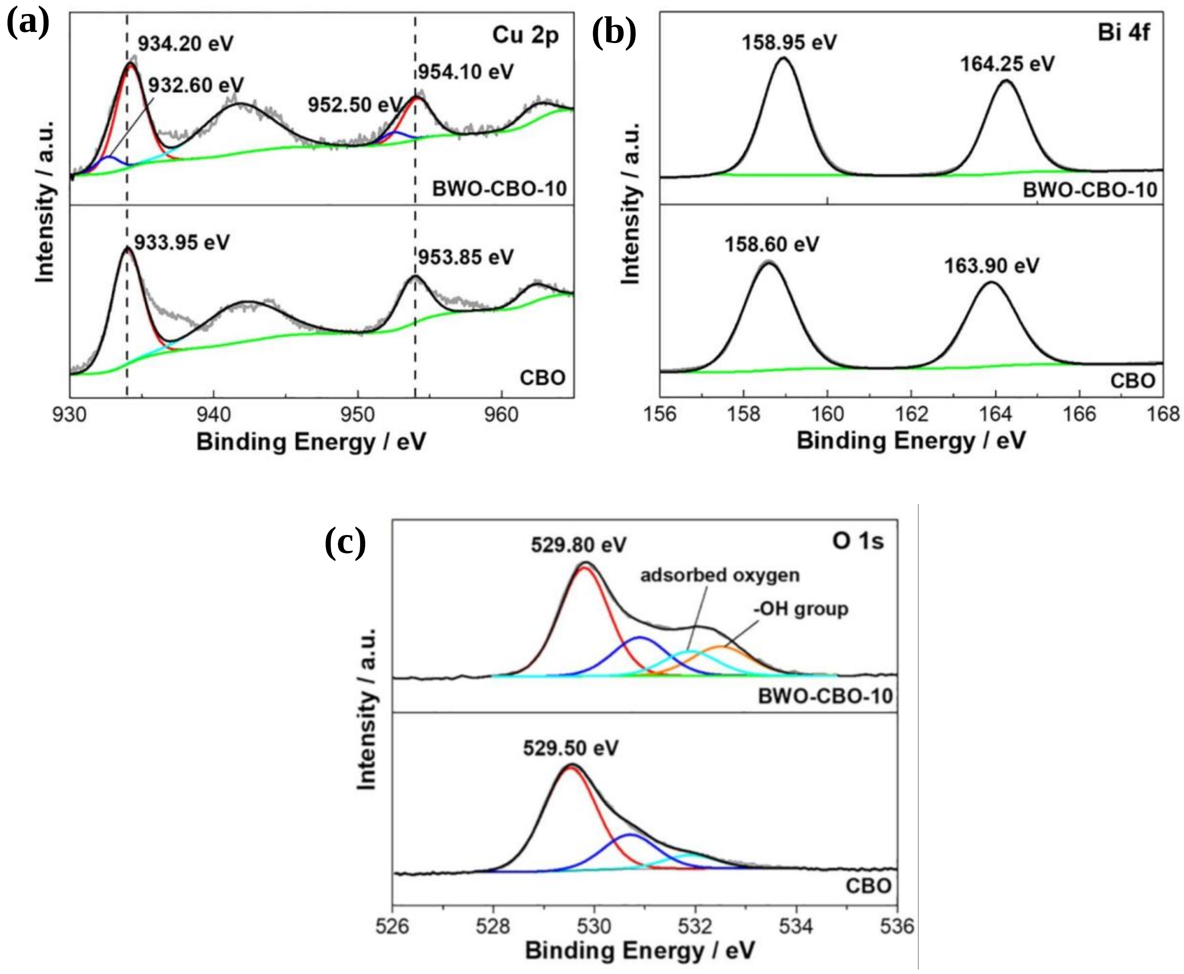

Fig. 8. XPS spectra of binary $Bi_2WO_6/CuBi_2O_4$ (BWO-CBO-10) and bare $CuBi_2O_4$ (CBO) photocatalysts: Cu 2p **(a)**, Bi 4f **(b)**, and O 1s **(c)**. Reproduced from Ref. [72], copyright 2019, with permission from Elsevier.

2.1.2. Band structure characterization and corresponding theoretical analysis

It should be pointed out that the Fermi level (E_f) positions of the heterojunction components have a significant effect on the bending mode of energy band and charge transfer direction between these components. The flat-band position (close to that of Fermi level equilibrium) could be obtained from Mott-Schottky plots using Eq. (1) [75]:

$$\frac{1}{C^2} = \frac{2}{A^2 e \varepsilon \varepsilon_0 N_A} \left(E - V_{fb} - \frac{k_B T}{e}\right) \qquad \text{Eq. (1)}$$

where, C (interfacial capacitance), e (electronic charge), N_A (carrier concentration), ε (dielectric constant of the semiconductor), ε_0 (permittivity of free space), A (electrode surface), E (applied potential), V_{fb} (falt-band potential), k_B (Boltzmann constant), and T (absolute temperature).

The V_{fb} could be estimated from the potential (E) intercept by plotting $1/C^2$ *vs* E. The positive/negative slope of the Mott-Schottky curve of semiconductors indicates n/p-type character. The V_{fb} is closer to CB for n-type semiconductors and to VB for p-type ones. Typically, in the heterojunction system, the electrons could migrate from the semiconductor of higher E_f to that of lower E_f, resulting in upward and downward band bending (at the side of high E_f and low E_f, respectively), forming a new equilibrated Fermi level, causing a shift in the flat-band position. This phenomenon controls the direction of the transfer of the photo-induced charge carriers (it could be confirmed by XPS analysis). Therefore, the Mott-Schottky measurements might help to prove the Z-scheme formation. For example, the Mott-Schottky analysis has indicated that both Bi_2WO_6 and g-C_3N_4 are n-type semiconductors (a positive slope in the Mott-Schottky curve, Fig. 9a-b), and the energy bands are shifted downward and upward, respectively (Fig. 9c), due to the transfer of electrons from g-C_3N_4 (V_{fb} = -1.03 eV) to Bi_2WO_6 (V_{fb} = 0.36 eV) [76]. Therefore, under irradiation the photogenerated electrons should migrate from the Bi_2WO_6 to g-C_3N_4, suggesting the Z-scheme mechanism, as shown in Fig. 9d.

It is worth to mention that the loading of metal and metal oxide could also be useful to confirm the charge carriers' transfer mechanism in the Z-scheme photocatalytic systems since it is known that metals and metal oxides are selectively deposited on the electron-rich and electron-deficient sites/components (easily confirmed by the microscopic investigations [77]). Unfortunately, there are no reports on selective deposition of metal/metal oxides on Bi_2WO_6–based Z-scheme photocatalytic systems.

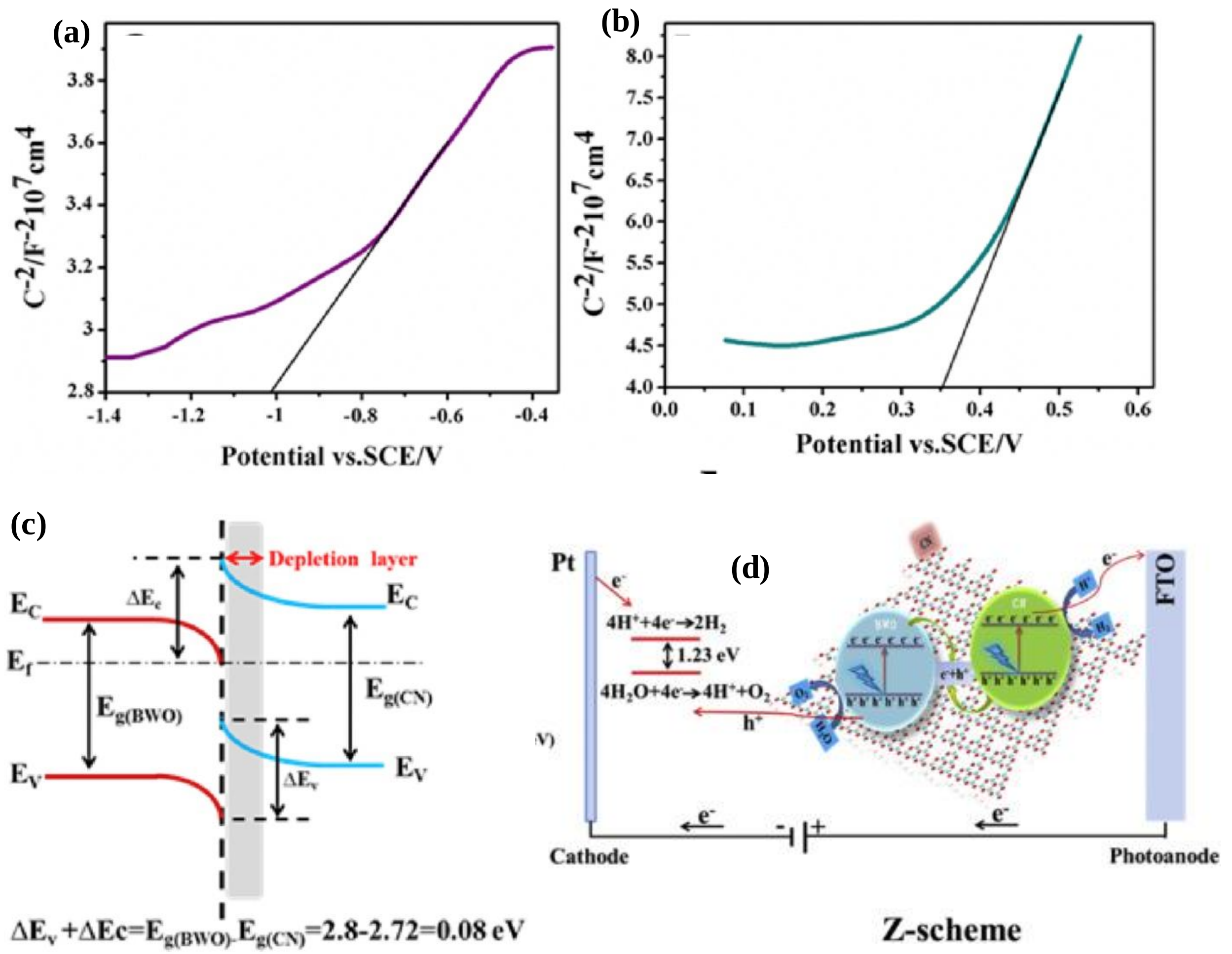

Fig. 9. (a-b) Mott-Schottky plots of $g\text{-}C_3N_4$ **(a)** and Bi_2WO_6 **(b)**, **(c)** the diagram of the band bending formed in the $Bi_2WO_6/g\text{-}C_3N_4$ hetrojunction, and **(d)** the schematic drawing for charge carriers' transfer in $Bi_2WO_6/g\text{-}C_3N_4$ Z-scheme. Reproduced from Ref. [76], copyright 2018, with permission from Elsevier.

Moreover, the theoretical simulations are significantly useful to estimate the mechanism of charge carriers' transfer in heterojunction systems. Usually, the first-principles simulation based on DFT calculation could be performed to evaluate the photogeneration and transfer of the charge carriers in a specific photocatalytic system by calculating the effective mass of charge carriers (m^*), as shown in Eq. (2) [77,78]:

$$m^* = \frac{\hbar}{\frac{d^2E_k}{dk^2}} \qquad \text{Eq. (2)}$$

where, m^* (effective mass of e^- or h^+), ħ (reduced Plank constant), k (wave vector), and E_k (energy corresponding to the wave vector).

It is worth noting that the charge carriers' migration (mobility) might be faster with decreasing the effective mass. For example, the theoretical simulation was used to confirm the formation of Bi_2WO_6/SnS Z-scheme photocatalytic system [78]. Firstly, the electronic-band structure of Bi_2WO_6 and SnS were estimated by using first-principles simulation based on DFT calculation, as shown in Figs. 10a-b. Thereafter, the effective masses of electrons and holes for Bi_2WO_6 and SnS were calculated. It has been found that the mobility of electrons (0.192) in Bi_2WO_6 is much higher than that in SnS (0.010), and hence the electrons would transfer from Bi_2WO_6 to SnS, resulting in Z-scheme mechanism, as shown in Fig. 10c.

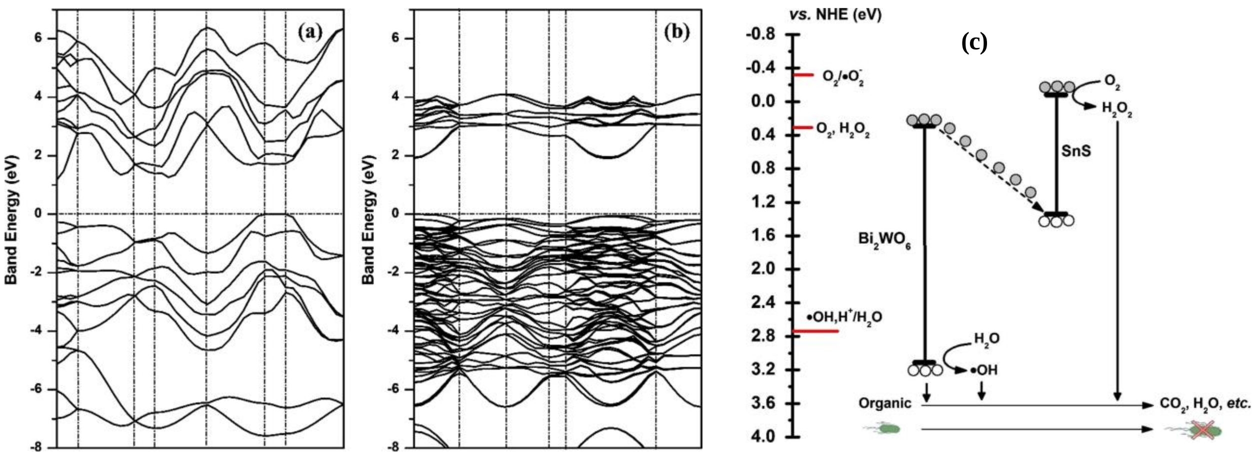

Fig. 10. (a-b) Band structure of SnS **(a)** and Bi_2WO_6 **(b)**, and **(c)** the diagram of charge carriers' transfer in the Bi_2WO_6/SnS Z-scheme photocatalyst. Reproduced from Ref. [78], copyright 2019, with permission from Elsevier.

Summarizing, it should be pointed out that despite various methods have been proposed for mechanism confirmation; many of them do not give the direct proof for Z-scheme migration of charge carriers. For example, the shift in XPS suggests only the strong interaction between components under dark conditions, which does not unequivocally confirm the direction of charge carriers` migration under irradiation. Therefore, it is proposed that in-situ methods under irradiation would be the most recommended, such as EPR studies.

Similarly, the comparison of properties of photocatalysts before and after irradiation might provide some insights on the mechanism of charge carriers' migration, e.g., the change of oxidation states of elements (by XPS as shown for other materials [79]). However, it should be pointed out that such changes should not be observed in perfectly stable materials, i.e., without photo-corrosion. The microscopic investigations for the selective deposition of metals and/or metal oxides on the surface of photocatalyst components with reductive and oxidative properties, respectively, might be also helpful, but it should be remembered that the presence of such deposits does not unequivocally prove their selective deposition during irradiation since the post-deposition migration towards the most stable component (adsorption-governed) must also be considered, as recently reported for faceted titania [80].

Scavenger tests and photoluminescence experiments might provide some insights on the possible direction of charge carriers, but all materials/components must be carefully analyzed (with reference experiments; not only for the most active sample), e.g., for ternary A/B/C photocatalyst, the activity for A, B, C, A/B, A/C, B/C and A/B/C should be compared.

It should be pointed out that though dyes are commonly used as testing molecules because of their convenient and cheap analysis (UV/vis), the sensitization of semiconductor by them should be included in the overall mechanism, which might be quite challenging without action spectrum analysis [81]. Additionally, special care should be taken for vis inactive components, e.g., TiO_2 and ZnO, since their vis response would be mainly caused by dye-sensitization mechanism (self-doping could also give vis activity), and thus other compounds (colorless) should be selected for activity testing instead of dyes [82]. Moreover, for reliable comparison of different materials, the same conditions of light absorption should be provided, i.e., at the maximum of photoabsorption (usually at 1-2 g/L of photocatalyst), as pointed by H. Kisch [83]. It is thought, that the following experiments might be useful to prove the Z-scheme mechanism: (i) action spectrum analysis, (ii) irradiation by two sources with different energy (to activate one or more components), (iii) light-intensity dependence, (iv) selective redox reactions (e.g., hydrogen generation on the photocatalyst containing of only one component able to reduce proton), and (v) in-situ characterization of photocatalyst properties under irradiation, e.g., EPR.

Accordingly, it might be concluded that still a lot of work must be done to prove the mechanism of Z-scheme charge carriers` migration for BWO-based materials using novel and powerful characterization tools. Furthermore, the advanced theoretical calculations and modeling are greatly needed for deeper understanding of the mechanism of charge carriers' transfer kinetics in the Z-scheme systems.

2.2. Applications of Bi_2WO_6-based photocatalysts

Based on the above-mentioned properties of BWO-based photocatalysts, including an efficient spatial separation of photogenerated e^-/h^+ pairs and good redox properties, the efficient solar-energy conversion for wide range applications has already been reported, including environmental purification, solar fuel generation, and photocatalytic organic synthesis, as briefly presented in the following sections.

2.2.1. Environmental purification

With the rapid industrial development and population growth, numerous harmful organic compounds (HOCs) enter the environment every day. These HOCs have negative impacts on humans, animals, plants, and even whole ecosystem. Therefore, efficient, cheap and green methods of HOCs removal must be applied worldwide. Although, physical methods, e.g., adsorption, filtration, coagulation, separation, flotation and air stripping, are quite efficient, the pollutants are not decomposed, but only moved to another form/state (e.g., water/wastewater/air → solid waste; water/wastewater → gas phase). Therefore, other methods based on decomposition of pollutants (preferably complete degradation – mineralization) are highly recommended, such as AOPs/AOTs (as discussed in section 1).

Accordingly, BWO-based photocatalysts have shown to be a perspective material for the decomposition of organic pollutants in water/wastewater, including dyes (methylene blue, methyl orange, methyl green, rhodamine B, reactive blue 19, basic blue 41, acid fuchsin, malachite green, auramine-O, crystal violet and procion Red MX-5B), phenolic compounds (phenol, bisphenol, 4-nitrophenol, 2,4-dichlorophenol, 2,4,6-trichlorophenol and pentachlorophenol), pharmaceuticals, personal care products and endocrine disruptors (tetracycline, oxytetracycline, metronidazole, salicylic acid, levofloxacin, norfloxacin, and ciprofloxacin, cephalexin, enrofloxacin, fluoroquinolones, glyphosate, chlorpyrifos, 2-mercaptobenzothiazole, 17 β-estradiol) [31-34,36-42,44,46,47,49,50-55,57,59,60,63-69,72,73,84-104] (see Table 1).

Table 1. Examples of Bi_2WO_6-based Z-scheme photocatalysts for degradation of environmental pollutants

Photocatalytic system (PS)		Electron mediator	Light source	Application	Activity	Ref.
PSI (reduction)	**PSII (oxidation)**					
g-C_3N_4	Bi_2WO_6	Ag	500 W-Xe lamp (full-spectrum)	rhodamine B degradation	η = 92%; K = 0.013 min^{-1} (150 min)	[32]
g-C_3N_4	Bi_2WO_6	Au	300 W-Xe lamp (UV-cut-off filter, λ >	rhodamine B degradation	η = 88.7%; K = 0.07 min^{-1} (30 min)	[36]

			400 nm)			
$g-C_3N_4$	Bi_2WO_6	Pt	500 W-Xe lamp (UV-cut-off filter, λ > 420 nm)	rhodamine B degradation	η = 100%; K = 0.067 min^{-1} (70 min)	[38]
BiOBr	Bi_2WO_6	Bi	350 W-Xe lamp (UV-cut-off filter, λ > 420 nm)	rhodamine B degradation	η = 98.02%; K = 0.046 min^{-1} (60 min)	[41]
$g-C_3N_4$	Bi_2WO_6	Zn	300-W Xe lamp (UV-cut-off filter, λ > 400 nm)	bisphenol A degradation	η = 93%; K = 0.021 min^{-1} (120 min)	[44]
$g-C_3N_4$	Bi_2WO_6	PPy	500-W Xe lamp (UV-cut-off filter, λ > 420 nm)	rhodamine B degradation	η = 98%; K = 0.04 min^{-1} (100 min)	[46]
AgBr	Bi_2WO_6	RGO	350 W-Xe lamp (UV-cut-off filter, λ > 420 nm)	tetracycline degradation	η = 84%; K = 0.052 min^{-1} (60 min)	[50]
TiO_2	Bi_2WO_6	CNT	350 W-Xe lamp (full-spectrum)	cephalexin degradation	η = 89.7% (100 min)	[54]
$g-C_3N_4$	Bi_2WO_6	Mxene (Ti_3C_2)	300-W Xe lamp (full-spectrum)	ciprofloxacin degradation	η = 87.4%; K = 0.058 min^{-1} (70 min)	[55]
$g-C_3N_4$	Bi_2WO_6	-	300 W-Xe lamp (UV-cut-off filter, λ > 420 nm)	17β-estradiol degradation	η = 100% (50 min)	[63]
ZnCdS	Bi_2WO_6	-	1K W Xe lamp (full-spectrum)	malachite green degradation	η = 94%; K = 0.0534 min^{-1} (50 min)	[86]
Bi_2WO_6	P25-TiO_2	-	300 W-Xe lamp (UV-cut-off filter, λ > 420 nm)	fluoroquinolones degradation	η = 80% (90 min)	[90]

For example, Li et al. reported the photodegradation of rhodamine B (RhB) under vis irradiation on the direct Z-scheme photocatalyst $Bi_2Fe_4O_9/Bi_2WO_6$ (BFWO, synthesized with different contents of $Bi_2Fe_4O_9$ (BFO)) [58]. In this work, 100 mL of aqueous suspension of photocatalyst (30 mg) and RhB (10 mg L^{-1}) was stirred for 30 min in the dark (adsorption/desorption equilibrium), and then irradiated using 300-W Xe lamp and UV cut-off filter (λ > 420 nm) as a vis irradiation source. It was found that the best composite photocatalyst (BFWO-7) decomposed RhB completely (100%, 0.0380 min^{-1}) leading to its mineralization (75.9% total carbon (TOC) removal), which was much higher than that by pristine $Bi_2Fe_4O_9$ (15.2%, 0.0015 min^{-1}, TOC=8.6%) and Bi_2WO_6 (62.5%, 0.0122 min^{-1}, TOC=36.9%), ~~respectively,~~ as shown in Fig. 11a. Additionally, the BFWO-7 photocatalyst showed much higher activity (ca. one order in magnitude) than other one-component photocatalysts, such as TiO_2, CdS, ZnO, and NiO (Fig. 11b), and good photostability during 5 cycles (Fig. 11c). Additionally, the effect of coexisting ions (i.e., Na^+, Cl^-, NO_3^-, SO_4^{2-}, and CO_3^{2-}) was also investigated (Fig. 11d). For this purpose, the model inorganic salts (NaCl, $NaNO_3$, Na_2SO_4, and Na_2CO_3) at concentration of 0.1 mol L^{-1} were used. It was found that NaCl and $NaNO_3$ displayed a negligible effect on RhB degradation, probably due to their neutrality. However, a decrease in RhB degradation efficiency might arise from the competition between sodium cation and dye molecule for the limited reactive sites on the photocatalyst surface. The lower degradation efficiency in the presence of NaCl than $NaNO_3$ could be caused by the ability of generation of hydroxyl radical ($^{\bullet}OH$) by the latter, and thus increasing the degradation of RhB. On the other hand, Na_2SO_4 and especially Na_2CO_3 showed negative effects, resulting from an increase in the pH value of the reaction environment. The significant inhibition of RhB degradation by Na_2CO_3 is caused by generation of CO_3^{2-} and HCO_3^- (the product of Na_2CO_3 hydrolysis) acting as hole scavengers.

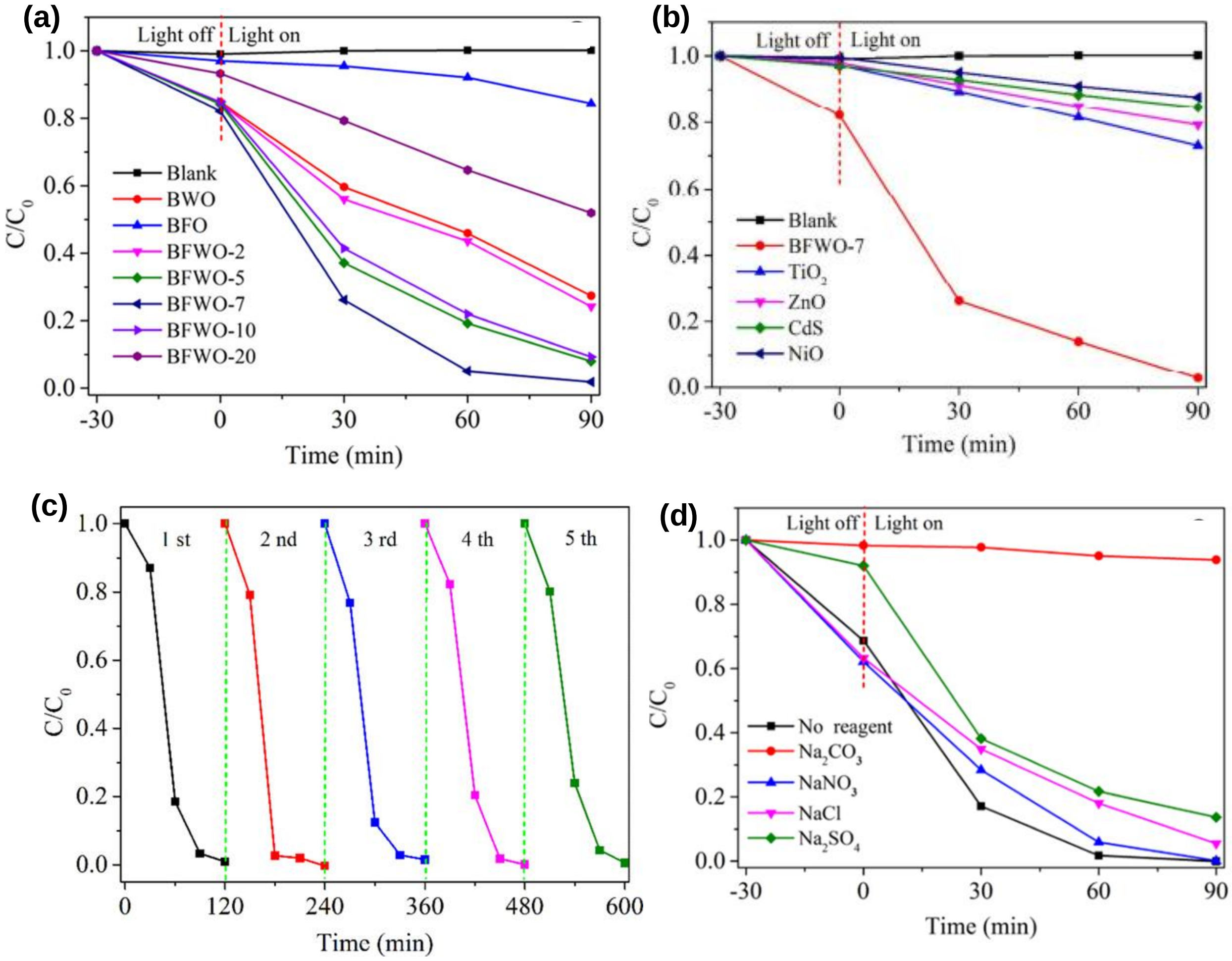

Fig. 11. (a) Photocatalytic activity of bare Bi_2WO_6 (BWO) and $Bi_2Fe_4O_9$ (BFO), and binary $Bi_2Fe_4O_9/Bi_2WO_6$ composites (BFWO) prepared with different BFO/BWO mass ratios, **(b)** comparative photocatalytic activity of BFWO-7 and conventional photocatalysts (TiO_2, ZnO, CdS and NiO), **(c)** reusability experiments of BFWO-7 photocatalyst for RhB (20 mg L^{-1}) degradation under vis irradiation, and **(d)** effect of coexisting ions on RhB degradation activity on BFWO-7 under vis irradiation. Reproduced from Ref. [58], copyright 2018, with permission from ACS.

In another study, the all-solid-state Z-scheme g-C_3N_4/RGO/Bi_2WO_6 photocatalyst (prepared with different contents of g-C_3N_4) showed to be highly efficient for photodegradation of 2,4,6-tricholorophenol (TCP) under vis irradiation [47]. In this report, 250 mL of aqueous suspension of photocatalyst (0.25 g) and TCP (20 mg L^{-1}) was stirred for 30 min in the dark, and then irradiated with 500-W Xe lamp and cut-off filter (420 nm) as a vis irradiation source. As shown in Fig. 12a, the composite photocatalyst (100% g-C_3N_4/RGO/Bi_2WO_6) exhibited much higher photocatalytic activity (98%) than its components (62% by binary g-C_3N_4/Bi_2WO_6 composite, and 58% and 52% for single photocatalysts, i.e., g-C_3N_4 and Bi_2WO_6, respectively) after 120-min vis irradiation. Moreover, high stability during five photodegradation cycles was also proven, as shown in Fig. 12b.

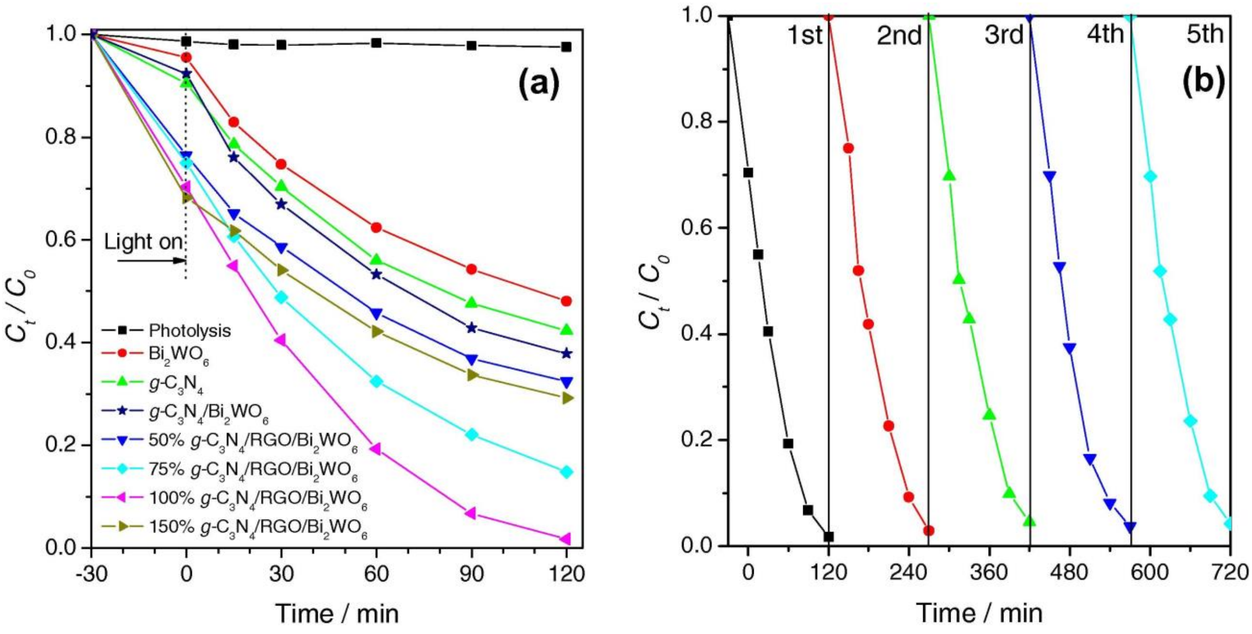

Fig. 12. Photocatalytic activity of Bi_2WO_6, g-C_3N_4, binary g-C_3N_4/Bi_2WO_6 composite, and ternary g-C_3N_4/RGO/Bi_2WO_6 composite, prepared with different contents of g-C_3N_4 for TCP degradation **(a)** and photocatalytic degradation cycles of TCP over g-C_3N_4/RGO/Bi_2WO_6 photocatalyst **(b)** under vis irradiation for 120 min. Reproduced from Ref. [47], copyright 2016, with permission from Elsevier.

Interestingly, two-dimensional (2D) Bi_2WO_6 exhibits higher photocatalytic activity than other morphologies, probably due to larger specific surface area and more photocatalytic active sites, greatly reducing the distance of charge transfer and facilitating the carrier migration from the interior to the photocatalyst surface. However, the photocatalytic activity of pure 2D Bi_2WO_6 is low (as clarified in Introduction), and thus 2D/2D materials have attracted much attention. Accordingly, Jiang et al. fabricated 2D/2D $SnNb_2O_6$/Bi_2WO_6 direct Z-scheme photocatalysts (with different contents of $SnNb_2O_6$) for photodegradation of antibiotic norfloxacin under vis irradiation [105]. In this study, the aqueous suspension of photocatalyst (50 mg) and norfloxacin (10 mg L^{-1}) was stirred for 30 min in the dark, and then irradiated using 300-W Xe lamp and UV cut-off filter (λ > 420 nm). The binary $SnNb_2O_6/Bi_2WO_6$ composite (3% $SnNb_2O_6/Bi_2WO_6$) exhibited the best activity, which was 9.3 and 2.3 times higher than its components ($SnNb_2O_6$ and Bi_2WO_6, respectively), as shown in Fig. 13a-b. Moreover, the high stability during four subsequent experiments was also proven (Fig. 13c).

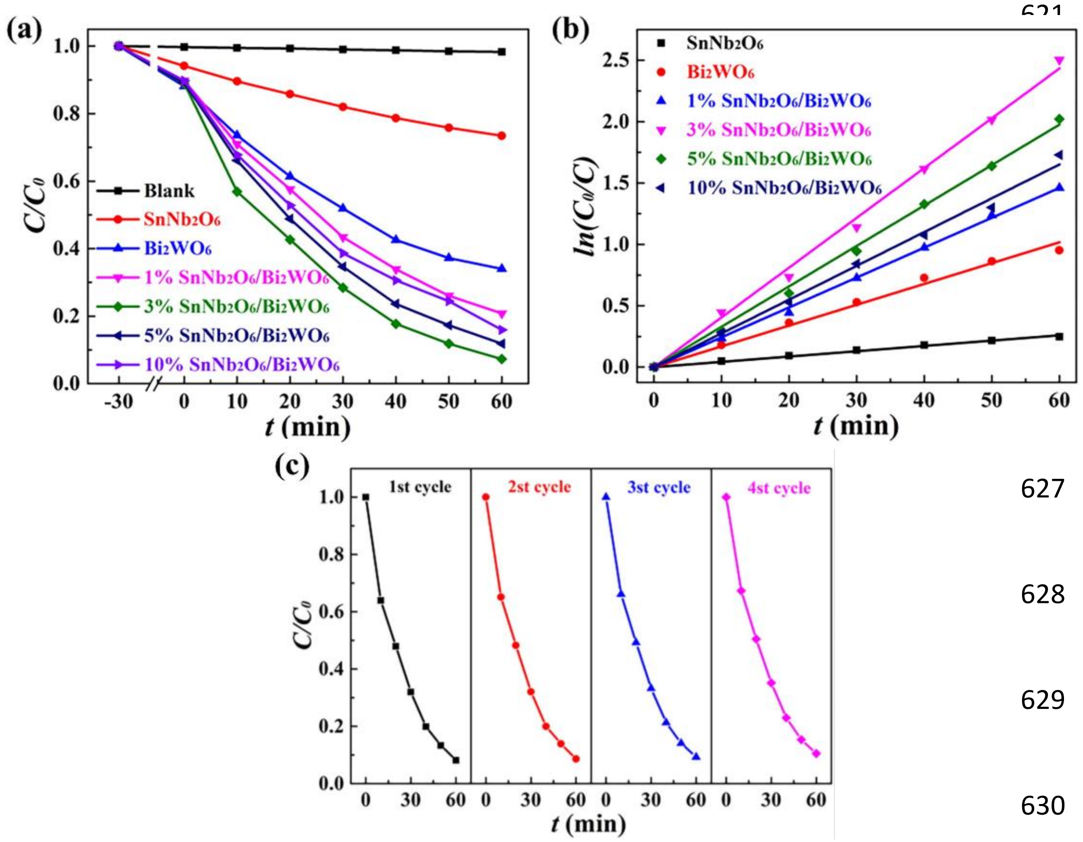

Fig. 13. (a-b) Photocatalytic degradation of norfloxacin over Bi_2WO_6, $SnNb_2O_6$, and $SnNb_2O_6/Bi_2WO_6$ composites (synthesized with different contents of $SnNb_2O_6$), under vis irradiation for 60 min **(a)** with the corresponding pseudo-first-order reaction kinetics **(b)**, and **(c)** the photodegradation cycles of norfloxacin over 3% $SnNb_2O_6/Bi_2WO_6$ Z-scheme. Reproduced from Ref. [105], copyright 2019, with permission from Elsevier.

Recently, great attention has been paid to the fabrication of metal-organic frameworks (MOFs) as a class of crystalline micro/mesoporous hybrid materials, composed of metal ions or metal clusters interconnected by organic linkers, because of their numerous structures and functions, which results in a new type of photoactive materials for diverse photocatalytic applications. More recently, nickel-based MOFs (Ni-MOFs), particularly 2D Ni-MOFs, have attracted intensive research interest because of their non-toxicity, low cost, different and tailored topological structures, and high stability [65]. Nevertheless, the bare Ni-MOFs showed low photocatalytic activity, because of the rapid recombination of photogenerated charges. The construction of Z-scheme from Ni-MOFs and other semiconductors of suitable energy bandgaps might be an effective strategy to solve this issue. Accordingly, Cheng et al. synthesized the direct Z-scheme of Bi_2WO_6/Ni-MOF sheets (NiBWO, with different compositions) for photodegradation of methylene blue (MB) dye under vis irradiation [65]. In this work, the aqueous suspension of photocatalyst (0.5 g) and MB (20 mg L^{-1}) was magnetically stirred for 30 min in the dark, and then irradiated with 300-W Xe lamp and UV cut-off filter (λ > 420 nm). It has been shown that the composite (NiBWO) could get 24- and 6.4-times higher activity than its components (Ni-MOF and BWO, respectively; Fig. 14a-b), reaching 91.1% removal of total organic carbon (TOC) during 30 h of irradiation (Fig. 14c).

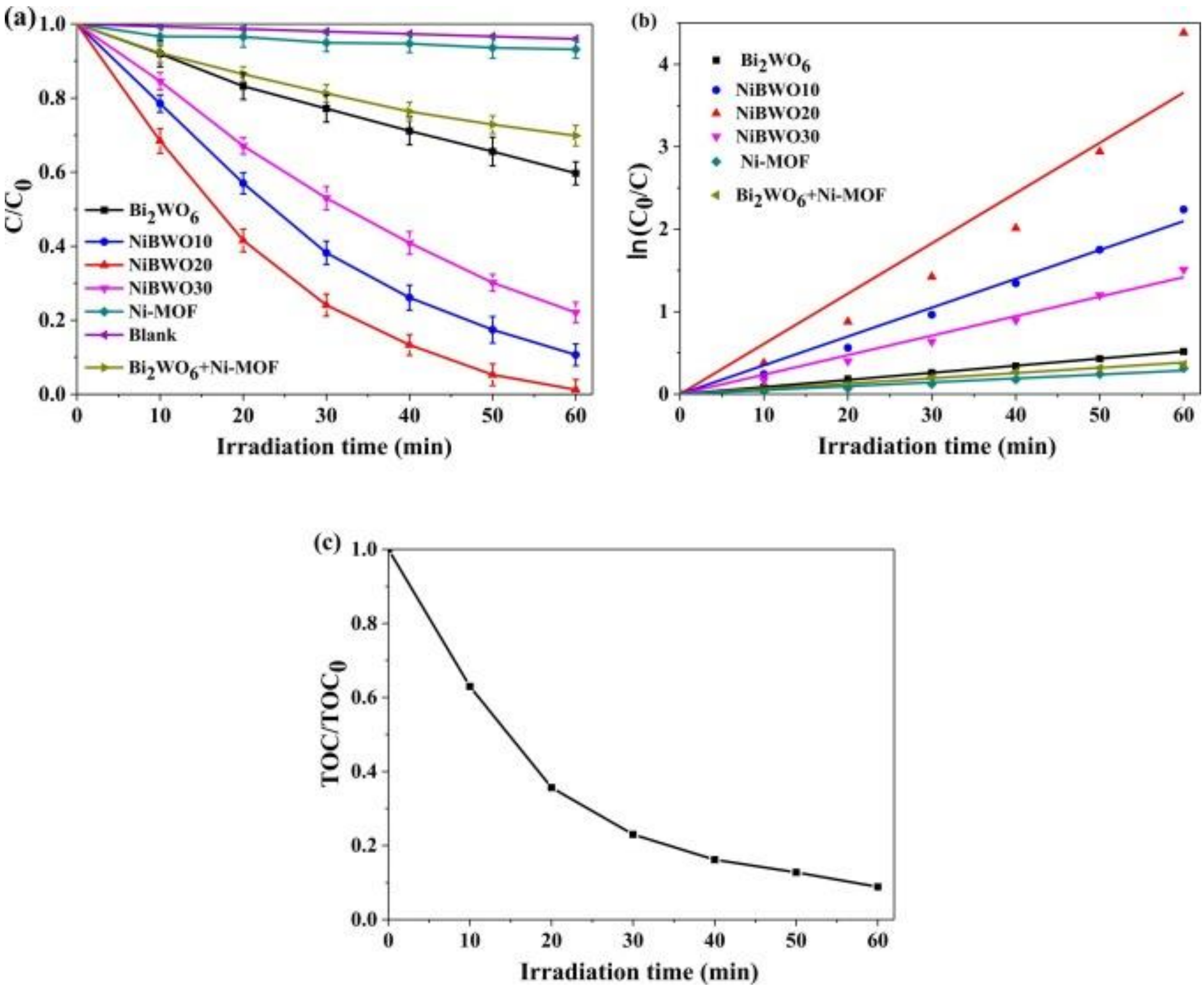

Fig. 14. (a-b) Photocatalytic degradation of MB over Bi_2WO_6, Ni-MOF, and NiBWO composites (synthesized with different contents of Ni-MOF: 10, 20, 30 wt.%), under vis irradiation for 60 min **(a)** with the corresponding pseudo-first-order reaction kinetics **(b)**, and **(c)** the TOC removal within MB degradation over NiBWO (20wt% of Ni-MOF) under vis irradiation [65]. Copyright 2022, with permission from Elsevier.

Summarizing, it is obvious that BWO-based Z-scheme photocatalysts have exhibited remarkable photocatalytic activity towards photodegradation of organic pollutants (dyes, phenolic compounds, pharmaceuticals and pesticide). However, the physicochemical characteristics of BWO-based Z-scheme photocatalyst should be further investigated. Additionally, the photocatalytic degradation mechanism of organic compounds and the combination of outstanding activity with photostability and reusability need further clarifications (only limited number of reports dealing with these aspects). Moreover, the design and operative optimization of BWO-based photocatalysis processes should be fully investigated, considering the effluent properties to enable the use of BWO-based Z-scheme photocatalytic systems at large scale (industrial scale) with high performance and low cost.

Another kind of pollutants, which has been treated by BWO-based photocatalyst, is the group of heavy metals. Although BWO-based Z-scheme photocatalysts have been suggested to be a future perspective for the removal of heavy metals, to date, only Cr removal has been reported [99,106-110]. For instance, Z-scheme Co_3O_2/Ag/Bi_2WO_6 photocatalyst was used for photocatalytic reduction of Cr(VI) in an aqueous phase under vis irradiation (300-W xenon lamp with UV cut-off filter, $\lambda > 420$ nm) [108]. Accordingly, it was found that the ternary photocatalyst (Co_3O_2/Ag/Bi_2WO_6) exhibited the best photocatalytic activity (58.0% (Fig. 15a), 0.0153 min^{-1} (Fig. 15b)), which was 1.3 and 2.1 times higher than those of the binary photocatalysts (Ag/Bi_2WO_6 (43.4%, 0.0102 min^{-1}) and (Co_3O_2/Bi_2WO_6 (27.5%, 0.00598 min^{-1}), respectively, and 3.4 times higher than that by the single photocatalyst (Bi_2WO_6 (16.9%, 0.00328 min^{-1}), during 60 min-vis irradiation, as shown in Fig. 15.

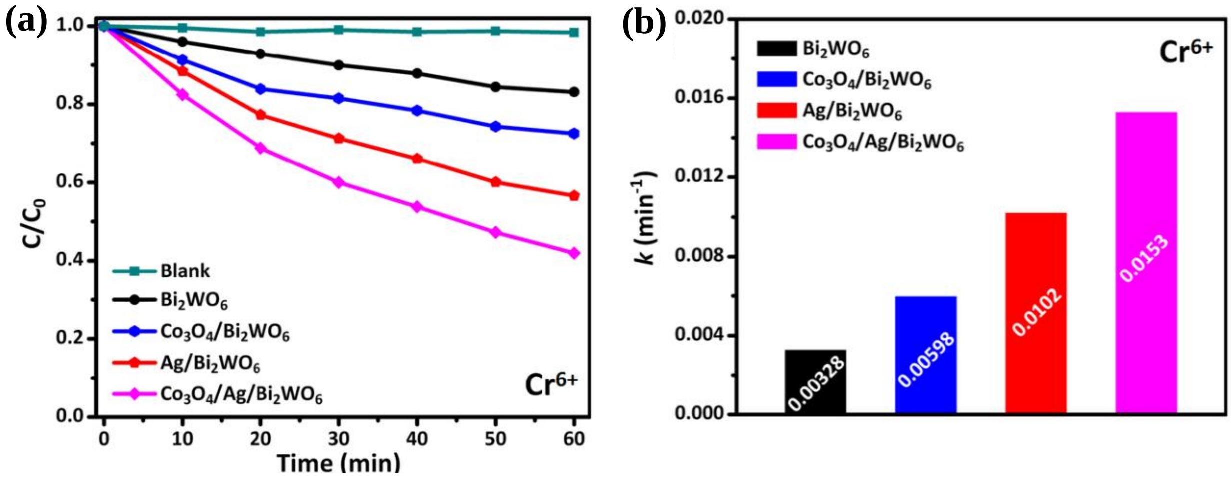

Fig. 15. Photocatalytic activity **(a)** and reaction rate constants **(b)** of Bi_2WO_6, Co_3O_2/Bi_2WO_6, Ag/Bi_2WO_6, and Co_3O_2/Ag/Bi_2WO_6 photocatalysts for removal of Cr^{6+} under vis irradiation. Reproduced from Ref. [108], copyright 2019, with permission from Elsevier.

BWO-based photocatalysts have also been proposed for removal of microorganisms from water/wastewater. However, only two studies by Li et al. [78], and Yang et al. [88] have been reported up to date [67]. For example, Li et al. reported photo-inactivation of *E. Coli K*-

12 on direct Z-scheme SnS/Bi_2WO_6 (SB) photocatalysts (with different contents of SnS) using 300-W halogen tungsten lamp (with UV cut-off filter, $\lambda > 410$ nm) [78]. It was found that there was no noticeable change in the cell survival ratio in the dark condition, demonstrating that "dark" cytotoxicity of the photocatalyst was negligible, whereas under irradiation, bacteria inactivation was significantly enhanced, especially in the presence of SB photocatalyst, as shown in Fig. 16a (Fig. 16b presents the photographs of cultured *E. coli* colonies collected at different time during photocatalytic disinfection process.). Although SnS/Bi_2WO_6 (0.50 SB) photocatalyst has exhibited the highest photocatalytic activity (survival ratio = 32%) as compared to its components (survival ratios on SnS and Bi_2WO_6 equal to 81% 50%), the inactivation rate is quite low, i.e., much lower than that by modified titania photocatalysts (in logarithmic scale [111-113]), and hence further improvements in antibacterial performance (and against other microorganisms) are necessary.

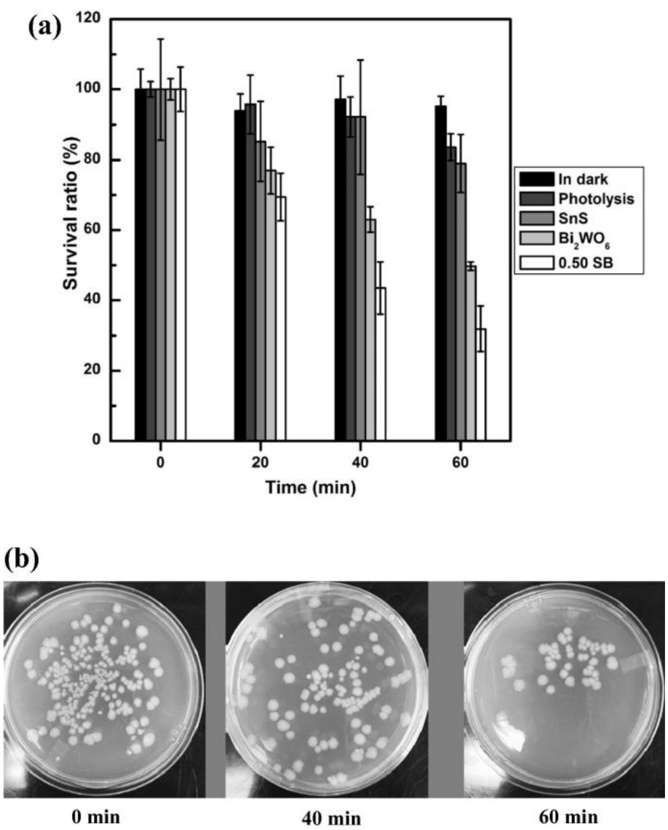

Fig. 16. Photocatalytic disinfection effect of SnS, Bi_2WO_6, and SnS/Bi_2WO_6 (0.05 SB) photocatalysts under vis irradiation **(a)** with photos of *E. coli* colonies, cultured by the samples collected at different time during photocatalytic disinfection process **(b)**. Reproduced from Ref. [78], copyright 2019, with permission from Elsevier.

Another application of BWO-based photocatalysts for environmental purification has been focused on air treatment [114-119]. For example, Hu et al. prepared Z-scheme 2D/2D black phosphorus/monolayer Bi_2WO_6 nanosheets (with different contents of black phosphorus (BP), coded as *x*% BP/MBWO, where *x* was the weight ratios of BP to MBWO) for photocatalytic removal of NO under vis irradiation (300-W Xe lamp and UV cut-off filter) [114]. It was found that Z-scheme BP/Bi_2WO_6 (12% BP/MBWO) photocatalyst possessed the best photocatalytic removal efficiency (61%), which was about 2.3-times higher than that of pristine Bi_2WO_6 (Fig. 17a), and good photostability even after six recycles (Fig. 17b).

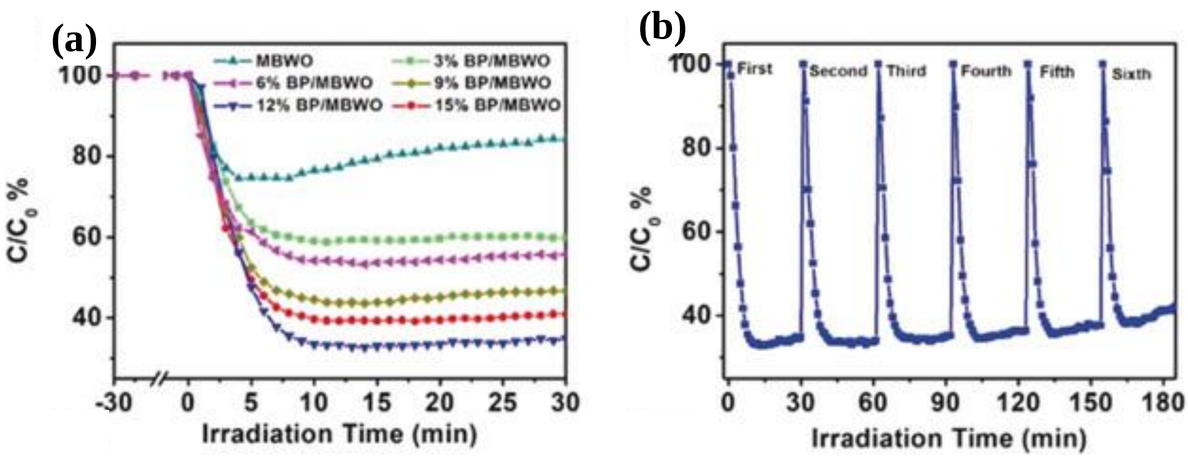

Fig. 17. Photocatalytic activity of monolayer Bi_2WO_6 (MBWO) and BP/MBWO (with different BP contents, 3−15%) for photo-removal of NO under vis irradiation **(a)**; and cyclic photocatalytic NO degradation reactions on 12% BP/MBWO **(b)**. Reproduced from Ref. [114], copyright 2019, with permission from Wiley.

Zhang et al. reported the UV photodegradation of gaseous benzene (as one of VOCs) over direct Z-scheme Bi_2WO_6/palygorskite photocatalyst (prepared with different loadings of palygorskite (Pa)) [115]. It was found that the Bi_2WO_6/Pa (8:2) composite exhibited the highest photocatalytic activity of 62.7%, which was much better than that by its components, i.e., 46.0% by Bi_2WO_6 and 35.8% by Pa.

In summary, though BWO-based photocatalysts have exhibited superior performance in comparison to their components towards photocatalytic removal of indoor air pollutants, this activity is still low, and hence more improvements are necessary for boosting the photocatalytic activity under vis irradiation. Moreover, there are only few reports dealing with photocatalytic removal of indoor air contaminants over BWO-based photocatalysts, and thus more study is highly needed.

2.2.2. Solar fuel generation

Among different Z-scheme photocatalytic systems, BWO-based photocatalysts have also been successfully used for H_2 generation [32,48,49,55,59,60,62,74,76,114,120,121]. For example, Qiang et al. reported the photocatalytic H_2-evolution over I-doped Z-scheme $Bi_2O_2CO_3/Bi_2WO_6$ photocatalyst (prepared with different contents of iodine) under vis irradiation (300-W Xe lamp, UV cut-off filter, $\lambda > 420$ nm) [62]. In this report, photocatalyst (25 mg) was dispersed into 50 mL aqueous suspension of methanol (10 vol%), and then stirred for 30 min in the dark. Before irradiation, the suspension was bubbled with argon to remove oxygen (an electron scavenger). It was found that the I-doped Z-scheme $Bi_2O_2CO_3/Bi_2WO_6$ photocatalyst (S5 sample) showed high stability (Fig. 18c) and best photocatalytic activity (186.22 μmol $g^{-1}h^{-1}$) when compared with non-doped $Bi_2O_2CO_3/Bi_2WO_6$ composite (S10 sample, 40.67 μmol $g^{-1}h^{-1}$), pristine $Bi_2O_2CO_3$ (S9 sample, 8.33 μmol $g^{-1}h^{-1}$) and bare Bi_2WO_6 (inactive S1), as shown in Fig. 18 a-b. Moreover, the addition of platinum (3 wt%) increased the photocatalytic activity of S5 sample by 3.6 times (664.5 μmol $g^{-1}h^{-1}$), reaching AQE of 14.9% (Fig. 18 a-b).

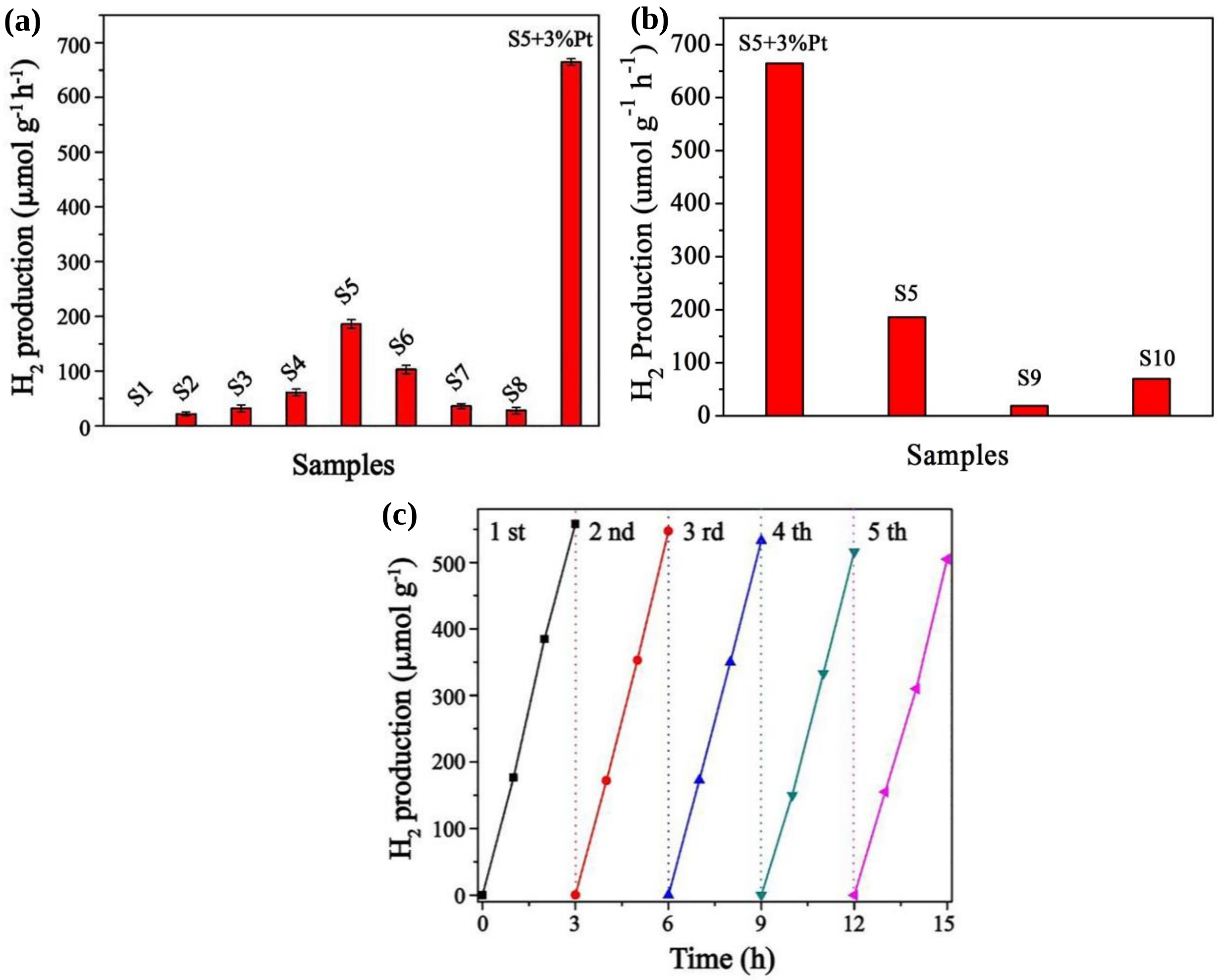

Fig. 18. (a-b) Photocatalytic activities of: Bi_2WO_6 (S1), and I-doped $Bi_2O_2CO_3/Bi_2WO_6$ photocatalysts, prepared with different contents of iodide (S2−S8) **(a)** and non-doped $Bi_2O_2CO_3/Bi_2WO_6$ (S10), I-doped $Bi_2O_2CO_3/Bi_2WO_6$ (S5), and bare $Bi_2O_2CO_3$ (S9) **(b)**, and **(c)** photocatalytic activity of I-doped $Bi_2O_2CO_3/Bi_2WO_6$ (S5) during 5-cycles. Reproduced from Ref. [62], copyright 2021, with permission from Elsevier.

Another example of direct Z-scheme photocatalyst was presented by Rauf et al. for overall water splitting into H_2 and O_2 under AM 1.5 G simulated solar light (100 mW cm^{-2}) on Bi_2WO_6/Cu_3P (prepared with different contents of Bi_2WO_6) photocatalyst [74]. The photocatalyst (100 mg) was dispersed into 80 mL of buffer aqueous suspension (0.5 M

Na_2HPO_4/NaH_2PO_4) and then bubbled with N_2. It was obvious that Bi_2WO_6 (30%)/Cu_3P composite exhibited the highest photocatalytic activity (H_2 = 9.3 μmol g^{-1}, O_2 = 4.6 μmol g^{-1}, H_2/O_2 ~ 2), when compared with bare Cu_3P (H_2 = 3.5 μmol g^{-1}, O_2 = 1.7 μmol g^{-1}) and pristine Bi_2WO_6 (no evolution of H_2 and O_2), as shown in Fig. 19a. Furthermore, the Z-scheme Bi_2WO_6 (30%)/Cu_3P photocatalyst exhibited good stability after 3-cycles photoreactions, as shown in Fig. 19b.

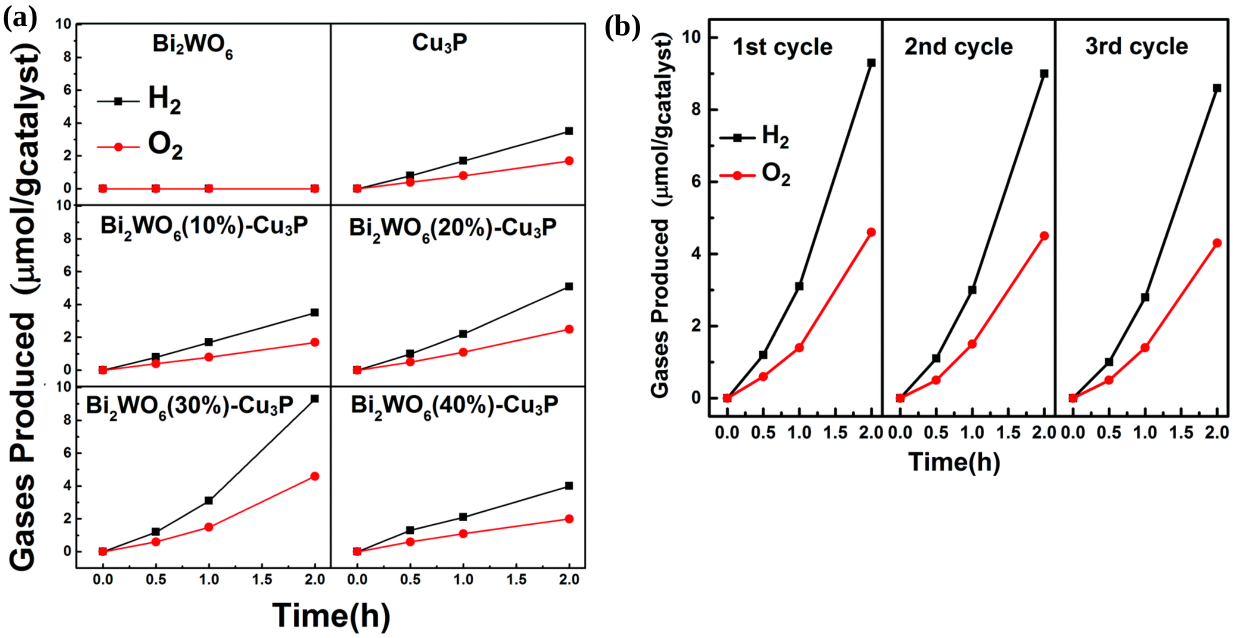

Fig. 19. (a) Time courses of photocatalytic overall water splitting on Bi_2WO_6, Cu_3P, and Bi_2WO_6/Cu_3P prepared with different Bi_2WO_6 contents (10−40%) under simulated solar light, and **(b)** reusability experiments for water splitting over Bi_2WO_6 (30%)/Cu_3P photocatalysts. Reproduced from Ref. [74], copyright 2018, with permission RSC.

Summarizing, it should be pointed out that though the fabrication of Z-scheme has enhanced the photocatalytic activity of Bi_2WO_6 for H_2 evolution and overall water splitting through the improvements of the charge carriers' separation and redox ability, and protecting Bi_2WO_6 against photocorrosion, the amounts of evolved gases are still low. Therefore, more studies are needed for activity improvements, especially in the absence of noble metal cocatalyst to decrease the operation cost.

Among solar-light-activated Z-scheme photocatalysts, BWO-based Z-scheme heterojunctions have also been fabricated for photocatalytic CO_2 reduction [35,43,48,56,122].

For example, Li et al. used direct Z-scheme g-C_3N_4/Bi_2WO_6 heterojunction (prepared with different contents of g-C_3N_4) for photoconversion of CO_2 into CO under vis irradiation (300-W xenon lamp, UV cut-off filter, λ > 420 nm) [56]. It was found that the g-C_3N_4/Bi_2WO_6 (prepared with addition of 0.1 g g-C_3N_4) exhibited the best photocatalytic activity with CO generation rate of 5.19 µmol g^{-1} h^{-1}, which was 22 and 6.4 times higher than those of bare g-C_3N_4 and Bi_2WO_6, respectively, as shown in Fig. 20. It should be pointed out, that though some BWO-based Z-scheme photocatalysts showed superior photocatalytic activity for photocatalytic conversion of CO_2 than its components, the selectivity, the mass transfer and thermodynamics of photocatalytic CO_2 reduction, as well as the reaction mechanism have not been well investigated yet, and thus further studies are needed.

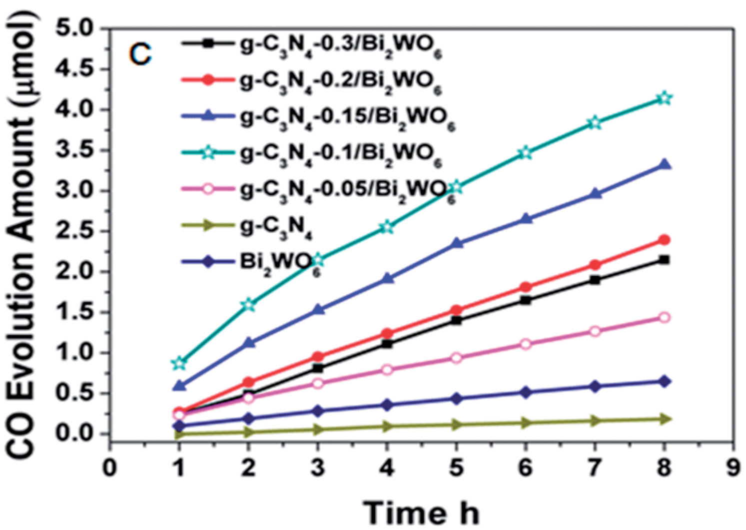

Fig. 20. Photocatalytic CO_2 reduction into CO on g-C_3N_4/Bi_2WO_6 heterojunctions prepared with different g-C_3N_4 contents, and pristine photocatalysts (g-C_3N_4 and Bi_2WO_6) under vis irradiation. Reproduced from Ref. [56], copyright 2015, with permission from RSC.

2.2.3. Organic synthesis

Among various Z-scheme photocatalytic systems, BWO-based photocatalysts have already been proposed also for photocatalytic organic synthesis. First and only one report on organic synthesis was shown for the photocatalytic selective conversion of 4-nitroaniline into 4-phenylenediamine by Yuan et al. over direct Z-scheme Bi_2WO_6/TiO_2 (prepared with different contents of BWO) and $Au@Bi_2WO_6/TiO_2$ under UV-vis irradiation (300-W xenon lamp, $320\ nm < \lambda < 780\ nm$) [120]. For photocatalytic reaction, 40 mL aqueous suspension of 4-nitroaniline (10 mg L^{-1}) containing 10 mg catalyst and 40 mg ammonium formate (as a hole scavenger) was stirred in dark for 2 h before illumination. It was found that the binary Bi_2WO_6/TiO_2 photocatalyst (prepared with 10 wt% of BWO) showed much higher photocatalytic activity (72% conversion) than its components, i.e., BWO (no activity) and TiO_2 (40% conversion), as shown in Fig. 21a. Additionally, Au (0.1 wt%) loaded on Z-scheme Bi_2WO_6/TiO_2 photocatalyst enhanced the activity to reach 100% conversion (Fig. 21b). Similar to other photocatalytic reactions, BWO-based photocatalyst exhibited good photostability during 5 reaction cycles, as presented in Fig. 21c. It should be noted that the BWO-based Z-scheme photocatalyst showed superior photocatalytic activity when compared to its components towards photoconversion of 4-nitroaniline into 4-phenylenediamine (which is essential industrial intermediate used for manufacturing different chemical compounds). Furthermore, the decoration with metal (Au) was a suitable strategy for boosting the activity of Z-scheme photocatalyst, resulting in complete conversion of 4-nitroaniline. However, the improvements for BWO-based Z-scheme photocatalytic system should be performed for vis response photocatalytic conversion processes.

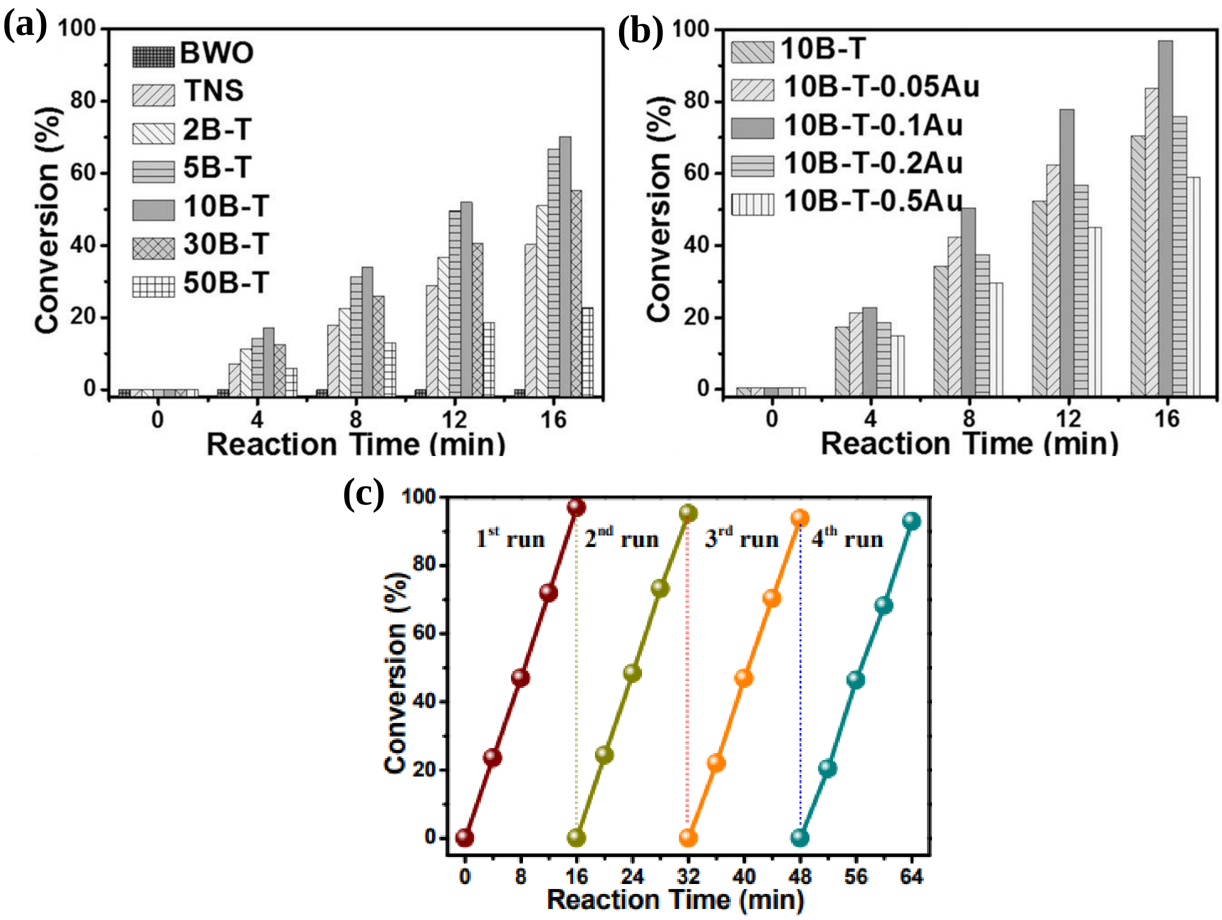

Fig. 21. (a-b) UV/vis photocatalytic conversion of 4-nitroaniline over: **(a)** bare TiO_2 (TNS) and BWO, and TiO_2/BWO composites prepared with different contents of BWO (2-50B–T) and **(b)** TiO_2/BWO loaded with different contents of Au (10B-T-0.05 to 0.5Au), and **(c)** recycling experiments over 10B-T-0.1Au. Reproduced from Ref. [120], copyright 2017, with permission from Wiley.

Summarizing, despite the heterogeneous photocatalysis is an effective method (green, sustainable and eco-friendly) for solar driven organic synthesis (through photocatalytic transformation), selectivity problems still limit the practical application. Therefore, it is essential to develop the synthetic methods, solvents (green and eco-friendly), as well as to improve the light absorption ability of the photocatalyst for low-cost photo-organic synthesis with high activity, stability and selectivity under vis irradiation. It should be pointed out that the activity of photocatalyst towards organic synthesis could also be improved by increasing the use of photogenerated charge carries and decreasing the use of scavengers by simultaneously selective photoreduction (by photogenerated electrons) and oxidation (by photogenerated holes) in one system. Moreover, it is significant to develop the photoreactor and in-situ detection methods for the photocatalytic organic synthesis to transform the synthesis from the lab-scale to large-scale industrial applications.

3. Summary and conclusions

Environmental pollution and energy shortage are considered as the biggest threats to human and every living organism in the world. Solar photocatalysis as green and clean technology is a promising strategy to resolve these issues. The main requirements, which determine the solar conversion efficiency of photocatalyst, are narrow bandgap (to widen the light-absorption range) and large bandgap (to achieve strong redox ability). However, these requirements are difficult to occur simultaneously in one-component photocatalyst. Therefore, great efforts have been paid to develop the efficient photocatalyst working under wide range of solar radiation. It should be pointed out that the Z-scheme photocatalyst outperforms type-II heterojunction materials because of strong redox ability since the photogenerated electrons and holes are more negative and more positive, respectively, and additionally spatially separated. Accordingly, the construction of Z-scheme photocatalytic systems is regarded as a promising approach to realize solar-light conversion because of their efficient light harvesting ability, effective separation (spatially separated reductive and oxidative active species) and transfer of photogenerated charges, and strong redox ability.

Here, the development of Z-scheme photocatalysts from 1st to 3rd generation has been presented. Accordingly, it is thought that the direct Z-scheme (3rd generation) photocatalysts are the most promising since the charge mediators are not required, and thus (i) the building cost of direct Z-scheme can be largely reduced, (ii) the migration of photogenerated electrons is faster, (iii) the backward reactions are prevented, and (iv) light-shielding effect does not occur. Moreover, the band bending, and electrical field formed in the direct Z-scheme system accelerate the transfer of low-energy electrons from CB of semiconductor with low-Fermi level to recombine with holes from VB of semiconductor with high-Fermi level, leaving the photogenerated high-energy electrons and holes to drive the photocatalytic reactions.

Recently, great attention has been paid to the fabrication of the direct visible-light-activated photocatalysts because of their outstanding activity. Among them, BWO is considered as one of highly promising materials because of its non-toxicity, low cost, and outstanding physicochemical characteristics (i.e., nonlinear dielectric susceptibility, ferroelectric piezoelectricity, pyroelectricity, catalytic behavior, modifiable morphology, strong oxidation power, and good photochemical stability). However, the photocatalytic activity of pristine BWO is low due to its weak reduction potential, poor light-absorption efficiency, low specific surface area, and rapid recombination of photogenerated charge carriers. Moreover, the impossibility of simultaneous strong redox ability (demanding wide bandgap) and broad light-harvesting efficiency (requiring narrow bandgap) is a big challenge for the practical application of pure BWO. Therefore, BWO-based Z-scheme photocatalysts have been constructed to overcome these shortcomings.

In this review, the recent developments on Z-scheme photocatalytic systems with special emphasis on the Bi_2WO_6-based photocatalysts, including the types, photocatalytic mechanisms and practical applications have been presented. It has been proven that BWO-based Z-scheme photocatalysts show high photocatalytic activity towards various applications, including environmental purification, solar energy generation, and photocatalytic synthesis of organic compounds. It should be pointed out that the morphology is also crucial, and thus some advanced structures (e.g., 2D/2D and core-shells) could facilitate the transfer and separation efficiency of photoinduced charge carriers, and hence boosting the activity of BWO-based Z-scheme photocatalysts. It should be pointed out that BWO-based Z-scheme photocatalysts have exhibited high vis activity for photocatalytic reduction of inorganic pollutants in water (heavy metals), air purification (greenhouse gases), degradation of organic compounds (in water and air), water splitting, and synthesis of organic compounds. However, the mechanisms of CO_2 conversion and decomposition of organic compounds need further clarification, i.e., Z-scheme mechanism is one of the solutions, but it should be pointed out that oxygen might be reduced in two-electron transfer mode, and thus high conduction-band bottom position is not required (as reported for pristine BWO [123-125]). Moreover, the antibacterial activity under vis irradiation is much lower than that by modified titania photocatalysts, and thus needs further improvements. To our knowledge, this is the first review on BWO-based Z-scheme photocatalysts to date, and it is thought it should be useful for scientific community to fully explore the potential of BWO-based Z-scheme photocatalysts for environmental remediation, energy conversion and organic synthesis.

Acknowledgements: T. M. Khedr acknowledges a scholarship from the Egyptian Government to Hokkaido University, Japan. A part of this study was financially supported from Polish National Science Centre (2016/21/B/ST5/03387) and "Yugo-Sohatsu Kenkyu" for an Integrated Research Consortium on Chemical Sciences (IRCCS) project from the Ministry of Education and Culture, Sport, Science and Technology-Japan (MEXT).

Conflict of interest: The authors declare no conflict of interest.

References

[1] M.A. Fox, M.T. Dulay, Heterogeneous Photocatalysis, Chemical Rev. 93 (1993) 341–357. https://doi.org/10.1021/cr00017a016.

[2] D.F. Ollis, E. Pelizzetti, N. Serpone, Photocatalyzed destruction of water contaminants, Environ. Sci. Technol. 25 (1991) 1522–1529. https://doi.org/10.1021/es00021a001.

[3] M.R. Hoffmann, S.T. Martin, W. Choi, D.W. Bahnemann, Environmental applications of semiconductor photocatalysis, Chem. Rev. 95 (1995) 69–96. https://doi.org/10.1021/cr00033a004.

[4] K. Wang, M. Janczarek, Z. Wei, T. Raja-Mogan, M. Endo-Kimura, T.M. Khedr, B. Ohtani, E. Kowalska, Morphology-and crystalline composition-governed activity of titania-based photocatalysts: Overview and perspective, Catalysts. 9 (2019) 1054. https://doi.org/10.3390/catal9121054.

[5] R. Abe, Recent progress on photocatalytic and photoelectrochemical water splitting under visible light irradiation, J. Photochem. Photobiol. C. 11 (2010) 179–209. https://doi.org/10.1016/j.jphotochemrev.2011.02.003.

[6] M. Tabata, K. Maeda, M. Higashi, D. Lu, T. Takata, R. Abe, K. Domen, Modified Ta_3N_5 Powder as a Photocatalyst for O_2 Evolution in a Two-Step Water Splitting System with an Iodate/Iodide Shuttle Redox Mediator under Visible Light, Langmuir. 26 (2010) 9161–9165. https://doi.org/10.1021/la100722w.

[7] V.K. Mrunal, A.K. Vishnu, N. Momin, J. Manjanna, Cu_2O nanoparticles for adsorption and photocatalytic degradation of methylene blue dye from aqueous medium, Environ. Nanotechnol. Monit. Manag. 12 (2019) 100265. https://doi.org/https://doi.org/10.1016/j.enmm.2019.100265.
[8] M.F.R. Samsudin, R. Bashiri, N.M. Mohamed, Y.H. Ng, S. Sufian, Tailoring the morphological structure of $BiVO_4$ photocatalyst for enhanced photoelectrochemical solar hydrogen production from natural lake water, Appl. Surf. Sci. 504 (2020) 144417. https://doi.org/10.1016/j.apsusc.2019.144417.
[9] A. Molkenova, S. Sarsenov, S. Atabaev, L. Khamkhash, T.S. Atabaev, Hierarchically-structured hollow CuO microparticles for efficient photo-degradation of a model pollutant dye under the solar light illumination, Environ. Nanotechnol. Monit. Manag. 16 (2021) 100507. https://doi.org/https://doi.org/10.1016/j.enmm.2021.100507.
[10] J. Schneider, M. Matsuoka, M. Takeuchi, J. Zhang, Y. Horiuchi, M. Anpo, D.W. Bahnemann, Understanding TiO_2 Photocatalysis: Mechanisms and Materials, Chem. Rev. 114 (2014) 9919–9986. https://doi.org/10.1021/cr5001892.
[11] S. Bai, J. Jiang, Q. Zhang, Y. Xiong, Steering charge kinetics in photocatalysis: Intersection of materials syntheses, characterization techniques and theoretical simulations, Chem. Soc. Rev. 44 (2015) 2893–2939. https://doi.org/10.1039/c5cs00064e.
[12] A. Kudo, Z-scheme photocatalyst systems for water splitting under visible light irradiation, MRS Bull. 36, (2011) 32–38. https://doi.org/10.1557/mrs.2010.3.
[13] Y. Tachibana, L. Vayssieres, J.R. Durrant, Artificial photosynthesis for solar water-splitting, Nat. Photonics. 6 (2012) 511–518. https://doi.org/10.1038/nphoton.2012.175.
[14] Y. Wang, H. Suzuki, J. Xie, O. Tomita, D.J. Martin, M. Higashi, D. Kong, R. Abe, J. Tang, Mimicking Natural Photosynthesis: Solar to Renewable H_2 Fuel Synthesis by Z-Scheme Water Splitting Systems, Chem. Rev. 118 (2018) 5201–5241. https://doi.org/10.1021/acs.chemrev.7b00286.
[15] P. Chen, H. Liu, W. Cui, S.C. Lee, L. Wang, F. Dong, Bi-based photocatalysts for light-driven environmental and energy applications: Structural tuning, reaction mechanisms, and challenges, EcoMat. 2 (2020) e12047. https://doi.org/https://doi.org/10.1002/eom2.12047.
[16] Y. Liu, B. Yang, H. He, S. Yang, X. Duan, S. Wang, Bismuth-based complex oxides for photocatalytic applications in environmental remediation and water splitting: A review, Sci. Total Environ. 804 (2022) 150215. https://doi.org/https://doi.org/10.1016/j.scitotenv.2021.150215.
[17] F. Amano, K. Nogami, B. Ohtani, Visible Light-Responsive Bismuth Tungstate Photocatalysts: Effects of Hierarchical Architecture on Photocatalytic Activity, J. Phys. Chem. C. 113 (2009) 1536–1542. https://doi.org/10.1021/jp808685m.
[18] L. Zhang, H. Wang, Z. Chen, P.K. Wong, J. Liu, Bi_2WO_6 micro/nano-structures: Synthesis, modifications and visible-light-driven photocatalytic applications, Appl. Catal. B. 106 (2011) 1–13. https://doi.org/https://doi.org/10.1016/j.apcatb.2011.05.008.
[19] Z. Zhu, S. Wan, Y. Zhao, Y. Qin, X. Ge, Q. Zhong, Y. Bu, Recent progress in Bi_2WO_6-Based photocatalysts for clean energy and environmental remediation: Competitiveness, challenges, and future perspectives, Nano Select. 2 (2021) 187–215. https://doi.org/https://doi.org/10.1002/nano.202000127.
[20] H. Okudera, Y. Sakai, K. Yamagata, H. Takeda, Structure of russellite (Bi_2WO_6): origin of ferroelectricity and the effect of the stereoactive lone electron pair on the structure, Acta Cryst. B. 74 (2018) 295–303. https://doi.org/10.1107/S2052520618006133.
[21] A.D. Rae, J.G. Thompson, R.L. Withers, Structure refinement of commensurately modulated bismuth tungstate, Bi_2WO_6, Acta Cryst. B. 47 (1991) 870–881. https://doi.org/10.1107/S0108768191008030.
[22] K.S. Knight, The crystal structure of russellite; a re-determination using neutron powder diffraction of synthetic Bi_2WO_6, Mineral. Mag. 56 (1992) 399–409. https://doi.org/10.1180/minmag.1992.056.384.13.
[23] N.A. McDowell, K.S. Knight, P. Lightfoot, Unusual High-Temperature Structural Behaviour in Ferroelectric Bi_2WO_6, Chem. Eur. J. 12 (2006) 1493–1499. https://doi.org/10.1002/chem.200500904.

[24] R.W. Wolfe, R.E. Newnahm, M.I. Kay, Crystal structure of Bi_2WO_6, Solid State Commun. 7 (1969) 1797–1801. https://doi.org/https://doi.org/10.1016/0038-1098(69)90288-9.

[25] K.S. Knight, The crystal structure of ferroelectric Bi_2WO_6 at 961 K, Ferroelectrics. 150 (1993) 319–330. https://doi.org/10.1080/00150199308211450.

[26] A. Watanabe, Y. Sekikawa, F. Izumi, An outline of the structure of new layered bismuth lanthanum tungstate, $Bi_{2-x}La_xWO_6$ (x = 0.4–1.1), J. Solid State Chem. 41 (1982) 138–142. https://doi.org/https://doi.org/10.1016/0022-4596(82)90194-3.

[27] P.S. Berdonosov, D.O. Charkin, V.A. Dolgikh, S.Y. Stefanovich, R.I. Smith, P. Lightfoot, $Bi_{2-x}Ln_xWO_6$: a novel layered structure type related to the Aurivillius phases, J. Solid State Chem. 177 (2004) 2632–2634. https://doi.org/https://doi.org/10.1016/j.jssc.2004.03.004.

[28] L. Feng, D. Yang, S. Gai, F. He, G. Yang, P. Yang, J. Lin, Single bismuth tungstate nanosheets for simultaneous chemo-, photothermal, and photodynamic therapies mediated by near-infrared light, Chem. Eng. J. 351 (2018) 1147–1158. https://doi.org/https://doi.org/10.1016/j.cej.2018.06.170.

[29] Z. Li, K. Wang, J. Zhang, Y. Chang, E. Kowalska, Z. Wei, Enhanced Photocatalytic Activity of Hierarchical Bi_2WO_6 Microballs by Modification with Noble Metals, Catalysts. 12 (2022) 130. https://doi.org/10.3390/catal12020130.

[30] M.T.L. Lai, C.W. Lai, K.M. Lee, S.W. Chook, T.C.K. Yang, S.H. Chong, J.C. Juan, Facile one-pot solvothermal method to synthesize solar active Bi_2WO_6 for photocatalytic degradation of organic dye, J. Alloys Compd. 801 (2019) 502–510. https://doi.org/https://doi.org/10.1016/j.jallcom.2019.06.116.

[31] L. Zhang, K.-H. Wong, Z. Chen, J.C. Yu, J. Zhao, C. Hu, C.-Y. Chan, P.-K. Wong, AgBr-Ag-Bi_2WO_6 nanojunction system: A novel and efficient photocatalyst with double visible-light active components, Appl. Catal. A. 363 (2009) 221–229. https://doi.org/https://doi.org/10.1016/j.apcata.2009.05.028.

[32] X. Xiao, J. Wei, Y. Yang, R. Xiong, C. Pan, J. Shi, Photoreactivity and Mechanism of g-C_3N_4 and Ag Co-Modified Bi_2WO_6 Microsphere under Visible Light Irradiation, ACS Sustainable Chem. Eng. 4 (2016) 3017–3023. https://doi.org/10.1021/acssuschemeng.5b01701.

[33] J. Huang, X. Li, G. Su, R. Gao, W. Wang, B. Dong, L. Cao, Construction of layer-by-layer g-C_3N_4/Ag/Bi_2WO_6 Z-scheme system with enhanced photocatalytic activity, J. Mater. Sci. 53 (2018) 16010–16021. https://doi.org/10.1007/s10853-018-2672-y.

[34] D. Huang, J. Li, G. Zeng, W. Xue, S. Chen, Z. Li, R. Deng, Y. Yang, M. Cheng, Facile construction of hierarchical flower-like Z-scheme AgBr/Bi_2WO_6 photocatalysts for effective removal of tetracycline: Degradation pathways and mechanism, Chem. Eng. J. 375 (2019) 121991. https://doi.org/https://doi.org/10.1016/j.cej.2019.121991.

[35] M. Wang, Q. Han, L. Li, L. Tang, H. Li, Y. Zhou, Z. Zou, Construction of an all-solid-state artificial Z-scheme system consisting of Bi_2WO_6/Au/CdS nanostructure for photocatalytic CO_2 reduction into renewable hydrocarbon fuel, Nanotechnology. 28 (2017) 274002. https://doi.org/10.1088/1361-6528/aa6bb5.

[36] Q. Li, M. Lu, W. Wang, W. Zhao, G. Chen, H. Shi, Fabrication of 2D/2D g-C_3N_4/Au/Bi_2WO_6 Z-scheme photocatalyst with enhanced visible-light-driven photocatalytic activity, Appl. Surf. Sci. 508 (2020) 144182. https://doi.org/10.1016/j.apsusc.2019.144182.

[37] Q. Wang, Q. Lu, L. Yao, K. Sun, M. Wei, E. Guo, Preparation and characterization of ultrathin Pt/CeO_2/Bi_2WO_6 nanobelts with enhanced photoelectrochemical properties, Dyes Pigm. 149 (2018) 612–619. https://doi.org/https://doi.org/10.1016/j.dyepig.2017.11.028.

[38] Y. Zhang, C. Chai, X. Zhang, J. Liu, D. Duan, C. Fan, Y. Wang, Construction of Pt-decorated g-C_3N_4/Bi_2WO_6 Z-scheme composite with superior solar photocatalytic activity toward rhodamine B degradation, Inorg. Chem. Commun. 100 (2019) 81–91. https://doi.org/https://doi.org/10.1016/j.inoche.2018.12.019.

[39] F. Yang, X. Zhu, J. Fang, D. Chen, W. Feng, Z. Fang, One step solvothermal synthesis of Bi/$BiPO_4$/Bi_2WO_6 heterostructure with oxygen vacancies for enhanced photocatalytic performance, Ceram. Int. 44 (2018) 6918–6925. https://doi.org/https://doi.org/10.1016/j.ceramint.2018.01.119.

[40] Y. Wang, X. Sun, T. Xian, G. Liu, H. Yang, Photocatalytic purification of simulated dye wastewater in different pH environments by using $BaTiO_3$/Bi_2WO_6 heterojunction

photocatalysts, Opt. Mater. 113 (2021) 110853. https://doi.org/10.1016/j.optmat.2021.110853.

[41] X. Chen, B. Zhao, J. Ma, L. Liu, H. Luo, W. Wang, The BiOBr/Bi/Bi_2WO_6 photocatalyst with SPR effect and Z-scheme heterojunction synergistically degraded RhB under visible light, Opt. Mater. 122 (2021) 111641. https://doi.org/10.1016/j.optmat.2021.111641.

[42] J. Jin, J. Sun, K. Lv, X. Guo, Q. Hou, J. Liu, J. Wang, Y. Bai, X. Huang, Oxygen vacancy BiO_{2-x}/Bi_2WO_6 synchronous coupling with Bi metal for phenol removal via visible and near-infrared light irradiation, J. Colloid Interface Sci. 605 (2022) 342–353. https://doi.org/10.1016/j.jcis.2021.06.085.

[43] Y. Wen Teh, Y. Wei Goh, X. Ying Kong, B. Ng, S. Yong, S. Chai, Fabrication of Bi_2WO_6/Cu/WO_3 All-Solid-State Z-Scheme Composite Photocatalyst to Improve CO_2 Photoreduction under Visible Light Irradiation, ChemCatChem. 11 (2019) 6431–6438. https://doi.org/10.1002/cctc.201901653.

[44] X. Ruan, Y. Hu, Effectively enhanced photodegradation of Bisphenol A by in-situ g-C_3N_4-Zn/Bi_2WO_6 heterojunctions and mechanism study, Chemosphere. 246 (2020) 125782. https://doi.org/https://doi.org/10.1016/j.chemosphere.2019.125782.

[45] Y. Zhang, Y. Zhao, Z. Xiong, R. Xiao, T. Gao, P. Liu, J. Liu, J. Zhang, Fabrication of Z-scheme VO-Bi_2WO_6/g-C_3N_4 heterojunction composite with visible-light-driven photocatalytic performance for elemental mercury removal, Chem. Eng. J. 425 (2021) 131537. https://doi.org/10.1016/j.cej.2021.131537.

[46] Z. Jiao, Y. Tang, P. Zhao, S. Li, T. Sun, S. Cui, L. Cheng, Synthesis of Z-scheme g-C_3N_4/PPy/Bi_2WO_6 composite with enhanced visible-light photocatalytic performance, Mater. Res. Bull. 113 (2019) 241–249. https://doi.org/https://doi.org/10.1016/j.materresbull.2019.02.016.

[47] D. Ma, J. Wu, M. Gao, Y. Xin, T. Ma, Y. Sun, Fabrication of Z-scheme g-C_3N_4/RGO/Bi_2WO_6 photocatalyst with enhanced visible-light photocatalytic activity, Chemi. Eng. J. 290 (2016) 136–146. https://doi.org/https://doi.org/10.1016/j.cej.2016.01.031.

[48] W.-K. Jo, S. Kumar, S. Eslava, S. Tonda, Construction of Bi_2WO_6/RGO/g-C_3N_4 2D/2D/2D hybrid Z-scheme heterojunctions with large interfacial contact area for efficient charge separation and high-performance photoreduction of CO_2 and H_2O into solar fuels, Appl. Catal. B. 239 (2018) 586–598. https://doi.org/https://doi.org/10.1016/j.apcatb.2018.08.056.

[49] H. Shen, G. Liu, Y. Zhao, D. Li, J. Jiang, J. Ding, B. Mao, H. Shen, K.-S. Kim, W. Shi, Artificial all-solid-state system by RGO bridged Cu_2O and Bi_2WO_6 for Z-scheme H_2 production and tetracycline degradation, Fuel. 259 (2020) 116311. https://doi.org/https://doi.org/10.1016/j.fuel.2019.116311.

[50] Z. Guan, X. Li, Y. Wu, Z. Chen, X. Huang, D. Wang, Q. Yang, J. Liu, S. Tian, X. Chen, AgBr nanoparticles decorated 2D/2D GO/Bi_2WO_6 photocatalyst with enhanced photocatalytic performance for the removal of tetracycline hydrochloride, Chem. Eng. J. 410 (2021) 128283. https://doi.org/10.1016/j.cej.2020.128283.

[51] R. Zhang, J. Yu, T. Zhang, C. Zhao, Q. Han, Y. Li, Y. Liu, K. Zeng, L. Cai, Z. Yang, Y. Ma, A novel snowflake dual Z-scheme Cu_2S/RGO/Bi_2WO_6 photocatalyst for the degradation of bisphenol A under visible light and its effect on crop growth, Colloids Surf. A Physicochem. Eng. Asp. 641 (2022) 128526. https://doi.org/https://doi.org/10.1016/j.colsurfa.2022.128526.

[52] D. Jiang, W. Ma, P. Xiao, L. Shao, D. Li, M. Chen, Enhanced photocatalytic activity of graphitic carbon nitride/carbon nanotube/Bi_2WO_6 ternary Z-scheme heterojunction with carbon nanotube as efficient electron mediator, J. Colloid Interface Sci. 512 (2018) 693–700. https://doi.org/https://doi.org/10.1016/j.jcis.2017.10.074.

[53] M. Li, C. Lai, H. Yi, D. Huang, L. Qin, X. Liu, B. Li, S. Liu, M. Zhang, Y. Fu, L. Li, J. He, Y. Zhang, L. Chen, Multiple charge-carrier transfer channels of Z-scheme bismuth tungstate-based photocatalyst for tetracycline degradation: Transformation pathways and mechanism, J. Colloid Interface Sci. 555 (2019) 770–782. https://doi.org/https://doi.org/10.1016/j.jcis.2019.08.035.

[54] F. Rabanimehr, M. Farhadian, A.R.S. Nazar, M. Moghadam, Fabrication of Z-scheme Bi_2WO_6/CNT/TiO_2 heterostructure with enhanced cephalexin photodegradation: Optimization and reaction mechanism, J. Mol. Liq. 339 (2021) 116728. https://doi.org/https://doi.org/10.1016/j.molliq.2021.116728.

[55] K. Wu, S. Song, H. Wu, J. Guo, L. Zhang, Facile synthesis of $Bi_2WO_6/C_3N_4/Ti_3C_2$ composite as Z-scheme photocatalyst for efficient ciprofloxacin degradation and H_2 production, Appl. Catal., A. 608 (2020) 117869. https://doi.org/https://doi.org/10.1016/j.apcata.2020.117869.
[56] M. Li, L. Zhang, X. Fan, Y. Zhou, M. Wu, J. Shi, Highly selective CO_2 photoreduction to CO over g-C_3N_4/Bi_2WO_6 composites under visible light, J. Mater. Chem. A. 3 (2015) 5189–5196. https://doi.org/10.1039/C4TA06295G.
[57] Z. Wang, T. Hu, K. Dai, J. Zhang, C. Liang, Construction of Z-scheme Ag_3PO_4/Bi_2WO_6 composite with excellent visible-light photodegradation activity for removal of organic contaminants, Chinese J. Catal. 38 (2017) 2021–2029. https://doi.org/https://doi.org/10.1016/S1872-2067(17)62942-5.
[58] B. Li, C. Lai, G. Zeng, L. Qin, H. Yi, D. Huang, C. Zhou, X. Liu, M. Cheng, P. Xu, C. Zhang, F. Huang, S. Liu, Facile Hydrothermal Synthesis of Z-Scheme $Bi_2Fe_4O_9/Bi_2WO_6$ Heterojunction Photocatalyst with Enhanced Visible Light Photocatalytic Activity, ACS Appl. Mater. Interfaces. 10 (2018) 18824–18836. https://doi.org/10.1021/acsami.8b06128.
[59] H. Yin, L. Yuting, M. Arif, Z. Min, X. Liu, A Bi_2WO_6-based hybrid heterostructures photocatalyst with enhanced photodecomposition and photocatalytic hydrogen evolution through Z-scheme process, J. Ind. Eng. Chem. 69 (2019) 345–357. https://doi.org/10.1016/j.jiec.2018.09.026.
[60] J. Zhang, J. Xin, C. Shao, X. Li, X. Li, S. Liu, Y. Liu, Direct Z-scheme heterostructure of p-$CuAl_2O_4$/n-Bi_2WO_6 composite nanofibers for efficient overall water splitting and photodegradation, J. Colloid Interface Sci. 550 (2019) 170–179. https://doi.org/https://doi.org/10.1016/j.jcis.2019.04.099.
[61] S. Li, J. Chen, S. Hu, H. Wang, W. Jiang, X. Chen, Facile construction of novel Bi_2WO_6/Ta_3N_5 Z-scheme heterojunction nanofibers for efficient degradation of harmful pharmaceutical pollutants, Chem. Eng. J. 402 (2020) 126165. https://doi.org/https://doi.org/10.1016/j.cej.2020.126165.
[62] Z. Qiang, X. Liu, F. Li, T. Li, M. Zhang, H. Singh, M. Huttula, W. Cao, Iodine doped Z-scheme $Bi_2O_2CO_3/Bi_2WO_6$ photocatalysts: Facile synthesis, efficient visible light photocatalysis, and photocatalytic mechanism, Chem. Eng. J. 403 (2021) 126327. https://doi.org/https://doi.org/10.1016/j.cej.2020.126327.
[63] Y. Qing, Y. Li, D. Hu, Z. Guo, Y. Yang, L. Geng, W. Li, 2D/2D Bi_2WO_6/Protonated g-C_3N_4 step-scheme heterojunctions for enhancing the photodegradation of 17β-estradiol: promotional role of electrostatic interaction, New J. Chem. 46 (2022) 2697–2709. https://doi.org/10.1039/D1NJ05334E.
[64] Y. Zeng, Q. Yin, Z. Liu, H. Dong, Attapulgite-interpenetrated g-C_3N_4/Bi_2WO_6 quantum-dots Z-scheme heterojunction for 2-mercaptobenzothiazole degradation with mechanism insight, Chem. Eng. J. 435 (2022) 134918. https://doi.org/https://doi.org/10.1016/j.cej.2022.134918.
[65] L. Cheng, M. Xie, Y. Sun, H. Liu, Bi2WO6-wrapped 2D Ni-MOF sheets with significantly improved photocatalytic activity by a direct Z-scheme electron transfer, J. Alloys Compd. 896 (2022) 163055. https://doi.org/https://doi.org/10.1016/j.jallcom.2021.163055.
[66] T. Chen, C. Xu, C. Zou, L. Fan, Q. Xu, Self-assembly of PDINH/TiO_2/Bi_2WO_6 nanocomposites for improved photocatalytic activity based on a rapid electron transfer channel, Appl. Surf. Sci. 584 (2022) 152667. https://doi.org/https://doi.org/10.1016/j.apsusc.2022.152667.
[67] L. Wang, Y. Liu, Y. Lin, X. Zhang, Y. Yu, R. Zhang, Z-scheme $Cu_2(OH)_3F$ nanosheets-decorated 3D Bi_2WO_6 heterojunction with an intimate hetero-surface contact through a hydrogen bond for enhanced photoinduced charge separation and transfer, Chem. Eng. J. 427 (2022) 131704. https://doi.org/https://doi.org/10.1016/j.cej.2021.131704.
[68] F. Du, Z. Lai, H. Tang, H. Wang, C. Zhao, Construction of dual Z-scheme Bi_2WO_6/g-C_3N_4/black phosphorus quantum dots composites for effective bisphenol A degradation, J Environ Sci (China). 124 (2023) 617–629. https://doi.org/https://doi.org/10.1016/j.jes.2021.10.027.
[69] Z. He, M.S. Siddique, H. Yang, Y. Xia, J. Su, B. Tang, L. Wang, L. Kang, Z. Huang, Novel Z-scheme In_2S_3/Bi_2WO_6 core-shell heterojunctions with synergistic enhanced photocatalytic degradation of tetracycline hydrochloride, J. Clean. Prod. 339 (2022) 130634.

https://doi.org/https://doi.org/10.1016/j.jclepro.2022.130634.

[70] M. Pelaez, N.T. Nolan, S.C. Pillai, M.K. Seery, P. Falaras, A.G. Kontos, P.S.M. Dunlop, J.W.J. Hamilton, J.A. Byrne, K. O'shea, A review on the visible light active titanium dioxide photocatalysts for environmental applications, Appl. Catal. B. 125 (2012) 331–349. https://doi.org/10.1016/j.apcatb.2012.05.036.

[71] S. Gligorovski, R. Strekowski, S. Barbati, D. Vione, Environmental Implications of Hydroxyl Radicals ($^{\bullet}OH$), Chem. Rev. 115 (2015) 13051–13092. https://doi.org/10.1021/cr500310b.

[72] X. Yuan, D. Shen, Q. Zhang, H. Zou, Z. Liu, F. Peng, Z-scheme $Bi_2WO_6/CuBi_2O_4$ heterojunction mediated by interfacial electric field for efficient visible-light photocatalytic degradation of tetracycline, Chem. Eng. J. 369 (2019) 292–301. https://doi.org/https://doi.org/10.1016/j.cej.2019.03.082.

[73] S. Sharma, A.O. Ibhadon, M.G. Francesconi, S.K. Mehta, S. Elumalai, S.K. Kansal, A. Umar, S. Baskoutas, Bi_2WO_6/C-Dots/TiO_2: A Novel Z-Scheme Photocatalyst for the Degradation of Fluoroquinolone Levofloxacin from Aqueous Medium, Nanomaterials. 10 (2020) 910. https://doi.org/10.3390/nano10050910.

[74] A. Rauf, M. Ma, S. Kim, M.S.A. Sher Shah, C.-H. Chung, J.H. Park, P.J. Yoo, Mediator- and co-catalyst-free direct Z-scheme composites of Bi_2WO_6–Cu_3P for solar-water splitting, Nanoscale. 10 (2018) 3026–3036. https://doi.org/10.1039/C7NR07952D.

[75] X. Lu, W. Che, X. Hu, Y. Wang, A. Zhang, F. Deng, S. Luo, D.D. Dionysiou, The facile fabrication of novel visible-light-driven Z-scheme $CuInS_2/Bi_2WO_6$ heterojunction with intimate interface contact by in situ hydrothermal growth strategy for extraordinary photocatalytic performance, Chem. Eng. J. 356 (2019) 819–829. https://doi.org/https://doi.org/10.1016/j.cej.2018.09.087.

[76] H. Hao, D. Lu, Q. Wang, Photoelectrochemical study on charge separation mechanisms of Bi_2WO_6 quantum dots decorated g-C3N4, Int. J. Hydrog. Energy. 43 (2018) 8824–8834. https://doi.org/https://doi.org/10.1016/j.ijhydene.2018.03.192.

[77] J. Low, S. Wageh, A.A. Al-Ghamdi, C. Jiang, B. Cheng, J. Yu, A Review of Direct Z-Scheme Photocatalysts, Small Methods. 1 (2017) 1700080. https://doi.org/10.1002/smtd.201700080.

[78] Z. Li, X. Meng, Z. Zhang, Hexagonal SnS nanoplates assembled onto hierarchical Bi_2WO_6 with enhanced photocatalytic activity in detoxification and disinfection, J. Colloid Interface Sci. 537 (2019) 345–357. https://doi.org/https://doi.org/10.1016/j.jcis.2018.10.070.

[79] K. Wang, Z. Bielan, M. Endo-Kimura, M. Janczarek, D. Zhang, D. Kowalski, A. Zielińska-Jurek, A. Markowska-Szczupak, B. Ohtani, E. Kowalska, On the mechanism of photocatalytic reactions on $Cu_xO@TiO_2$ core–shell photocatalysts, J. Mater. Chem. A. 9 (2021) 10135–10145. https://doi.org/10.1039/D0TA12472A.

[80] K. Kobayashi, M. Takashima, M. Takase, B. Ohtani, Mechanistic Study on Facet-Dependent Deposition of Metal Nanoparticles on Decahedral-Shaped Anatase Titania Photocatalyst Particles, Catalysts. 8 (2018) 542. https://doi.org/10.3390/catal8110542.

[81] X. Yan, T. Ohno, K. Nishijima, R. Abe, B. Ohtani, Is methylene blue an appropriate substrate for a photocatalytic activity test? A study with visible-light responsive titania, Chem. Phys. Lett. 429 (2006) 606–610. https://doi.org/https://doi.org/10.1016/j.cplett.2006.08.081.

[82] B. Ohtani, Photocatalysis A to Z—What we know and what we do not know in a scientific sense, J. Photochem. Photobiol., C. 11 (2010) 157–178. https://doi.org/https://doi.org/10.1016/j.jphotochemrev.2011.02.001.

[83] H. Kisch, On the Problem of Comparing Rates or Apparent Quantum Yields in Heterogeneous Photocatalysis, Angew. Chem., Int. Ed. 49 (2010) 9588–9589. https://doi.org/doi:10.1002/anie.201002653.

[84] R. Karuppannan, S. Mohan, T.-O. Do, Amine-functionalized metal–organic framework integrated bismuth tungstate (Bi_2WO_6/NH_2-UiO-66) composite for the enhanced solar-driven photocatalytic degradation of ciprofloxacin molecules, New J. Chem. 45 (2021) 22650–22660. https://doi.org/10.1039/D1NJ03977F.

[85] Y. Shao, X. Jin, C. Li, Y. Zheng, An effective non-equivalent ion exchange method for building an advanced Z-scheme WO_3/Bi_2WO_6 photocatalyst, New J. Chem. 45 (2021) 21863–21868. https://doi.org/10.1039/D1NJ03770F.

[86] X. Zhao, Y. Xu, X. Wang, Q. Liang, M. Zhou, S. Xu, Z. Li, Construction and enhanced

efficiency of Z-scheme-based $ZnCdS/Bi_2WO_6$ composites for visible-light-driven photocatalytic dye degradation, J Phys Chem Solids. 154 (2021) 110075. https://doi.org/https://doi.org/10.1016/j.jpcs.2021.110075.

[87] H. Bi, J. Liu, Z. Wu, K. Zhu, H. Suo, X. Lv, Y. Fu, R. Jian, Z. Sun, Construction of $Bi_2WO_6/ZnIn_2S_4$ with Z-scheme structure for efficient photocatalytic performance, Chem. Phys. Lett. 769 (2021) 138449. https://doi.org/https://doi.org/10.1016/j.cplett.2021.138449.

[88] P. Yang, C. Chen, D. Wang, H. Ma, Y. Du, D. Cai, X. Zhang, Z. Wu, Kinetics, reaction pathways, and mechanism investigation for improved environmental remediation by 0D/3D $CdTe/Bi_2WO_6$ Z-scheme catalyst, Appl. Catal. B. 285 (2021) 119877. https://doi.org/https://doi.org/10.1016/j.apcatb.2021.119877.

[89] A. Bahadoran, M. Farhadian, G. Hoseinzadeh, Q. Liu, Novel flake-like Z-Scheme Bi_2WO_6-$ZnBi_2O_4$ heterostructure prepared by sonochemical assisted hydrothermal procedures with enhanced visible-light photocatalytic activity, J. Alloys Compd. 883 (2021) 160895. https://doi.org/https://doi.org/10.1016/j.jallcom.2021.160895.

[90] J. Tian, L. Wei, Z. Ren, J. Lu, J. Ma, The facile fabrication of Z-scheme Bi_2WO_6-P25 heterojunction with enhanced photodegradation of antibiotics under visible light, J. Environ. Chem. Eng. 9 (2021) 106167. https://doi.org/https://doi.org/10.1016/j.jece.2021.106167.

[91] R. Zhang, K. Zeng, A novel flower-like dual Z-scheme $BiSI/Bi_2WO_6/g\text{-}C_3N_4$ photocatalyst has excellent photocatalytic activity for the degradation of organic pollutants under visible light, Diamond Relat. Mater. 115 (2021) 108343. https://doi.org/https://doi.org/10.1016/j.diamond.2021.108343.

[92] C. Piao, L. Chen, Z. Liu, J. Tang, Y. Liu, Y. Lin, D. Fang, J. Wang, Construction of solar light-driven dual Z-scheme $Bi_2MoO_6/Bi_2WO_6\backslash AgI\backslash Ag$ photocatalyst for enhanced simultaneous degradation and conversion of nitrogenous organic pollutants, Sep. Purif. Technol. 274 (2021) 119140. https://doi.org/10.1016/j.seppur.2021.119140.

[93] H.M. Aliabadi, K. Zargoosh, M. Afshari, M. Dinari, M.H. Maleki, Synthesis of a luminescent $g\text{-}C_3N_4–WO_3–Bi_2WO_6/SrAl_2O_4:Eu^{2+},Dy^{3+}$ nanocomposite as a double Z-scheme sunlight activable photocatalyst, New J. Chem. 45 (2021) 4843–4853. https://doi.org/10.1039/D0NJ05529H.

[94] X. Zheng, Y. Chu, B. Miao, J. Fan, Ag-doped $Bi_2WO_6/BiOI$ heterojunction used as photocatalyst for the enhanced degradation of tetracycline under visible-light and biodegradability improvement, J. Alloys Compd. 893 (2022) 162382. https://doi.org/https://doi.org/10.1016/j.jallcom.2021.162382.

[95] H. Jiang, Y. Li, X. Wang, X. Hong, Construction of a hydrangea-like $Bi_2WO_6/BiOCl$ composite as a high-performance photocatalyst, New J. Chem. 46 (2022) 2627–2634. https://doi.org/10.1039/D1NJ05409K.

[96] P. Zhao, B. Jin, Q. Zhang, R. Peng, Fabrication of $g\text{-}C_3N_4/Bi_2WO_6$ as a direct Z-scheme excellent photocatalyst, New J. Chem. 46 (2022) 5751–5760. https://doi.org/10.1039/D1NJ06034A.

[97] G. Kumar, R.K. Dutta, Fabrication of plate-on-plate SnS_2/Bi_2WO_6 nanocomposite as photocatalyst for sunlight mediated degradation of antibiotics in aqueous medium, J Phys Chem Solids. 164 (2022) 110639. https://doi.org/https://doi.org/10.1016/j.jpcs.2022.110639.

[98] Z. Ni, Y. Shen, L. Xu, G. Xiang, M. Chen, N. Shen, K. Li, K. Ni, Facile construction of 3D hierarchical flower-like Ag_2WO_4/Bi_2WO_6 Z-scheme heterojunction photocatalyst with enhanced visible light photocatalytic activity, Appl. Surf. Sci. 576 (2022) 151868. https://doi.org/https://doi.org/10.1016/j.apsusc.2021.151868.

[99] C. Lu, D. Yang, L. Wang, S. Wen, D. Cao, C. Tu, L. Gao, Y. Li, Y. Zhou, W. Huang, Facile construction of CoO/Bi_2WO_6 p-n heterojunction with following Z-Scheme pathways for simultaneous elimination of tetracycline and Cr(VI) under visible light irradiation, J. Alloys Compd. 904 (2022) 164046. https://doi.org/https://doi.org/10.1016/j.jallcom.2022.164046.

[100] C. Liu, H. Dai, C. Tan, Q. Pan, F. Hu, X. Peng, Photo-Fenton degradation of tetracycline over Z-scheme $Fe\text{-}g\text{-}C_3N_4/Bi_2WO_6$ heterojunctions: Mechanism insight, degradation pathways and DFT calculation, Appl. Catal. B. 310 (2022) 121326. https://doi.org/https://doi.org/10.1016/j.apcatb.2022.121326.

[101] Y. Liu, J. He, Y. Qi, Y. Wang, F. Long, M. Wang, Preparation of flower-like $BiOBr/Bi_2WO_6$

Z-scheme heterojunction through an ion exchange process with enhanced photocatalytic activity, Mater Sci Semicond Process. 137 (2022) 106195. https://doi.org/https://doi.org/10.1016/j.mssp.2021.106195.

[102] F. Zhao, D. Gao, X. Zhu, Y. Dong, X. Liu, H. Li, Rational design of multifunctional C/N-doped ZnO/Bi_2WO_6 Z-scheme heterojunction for efficient photocatalytic degradation of antibiotics, Appl. Surf. Sci. 587 (2022) 152780. https://doi.org/https://doi.org/10.1016/j.apsusc.2022.152780.

[103] S. Rajendran, T. Chellapandi, V. UshaVipinachandran, D. Venkata Ramanaiah, C. Dalal, S.K. Sonkar, G. Madhumitha, S.K. Bhunia, Sustainable 2D Bi_2WO_6/g-C_3N_5 heterostructure as visible light-triggered abatement of colorless endocrine disruptors in wastewater, Appl. Surf. Sci. 577 (2022) 151809. https://doi.org/https://doi.org/10.1016/j.apsusc.2021.151809.

[104] M. Su, H. Sun, Z. Tian, Z. Zhao, P. Li, Z-scheme 2D/2D WS_2/Bi_2WO_6 heterostructures with enhanced photocatalytic performance, Appl. Catal. A: Gen. 631 (2022) 118485. https://doi.org/https://doi.org/10.1016/j.apcata.2022.118485.

[105] R. Jiang, G. Lu, Z. Yan, D. Wu, J. Liu, X. Zhang, Enhanced photocatalytic activity of a hydrogen bond-assisted 2D/2D Z-scheme $SnNb_2O_6$/Bi_2WO_6 system: Highly efficient separation of photoinduced carriers, J. Colloid Interface Sci. 552 (2019) 678–688. https://doi.org/https://doi.org/10.1016/j.jcis.2019.05.104.

[106] Z. Lv, H. Zhou, H. Liu, B. Liu, M. Liang, H. Guo, Controlled assemble of oxygen vacant CeO_2@Bi_2WO_6 hollow magnetic microcapsule heterostructures for visible-light photocatalytic activity, Chem. Eng. J. 330 (2017) 1297–1305. https://doi.org/https://doi.org/10.1016/j.cej.2017.08.074.

[107] K. Kadeer, Y. Tursun, T. Dilinuer, K. Okitsu, A. Abulizi, Sonochemical preparation and photocatalytic properties of CdS QDs /Bi_2WO_6 3D heterojunction, Ceram. Int. 44 (2018) 13797–13805. https://doi.org/https://doi.org/10.1016/j.ceramint.2018.04.223.

[108] J. Wan, P. Xue, R. Wang, L. Liu, E. Liu, X. Bai, J. Fan, X. Hu, Synergistic effects in simultaneous photocatalytic removal of Cr(VI) and tetracycline hydrochloride by Z-scheme Co_3O_4/Ag/Bi_2WO_6 heterojunction, Appl. Surf. Sci. 483 (2019) 677–687. https://doi.org/https://doi.org/10.1016/j.apsusc.2019.03.246.

[109] Q. Zhang, M. Wang, M. Ao, Y. Luo, A. Zhang, L. Zhao, L. Yan, F. Deng, X. Luo, Solvothermal synthesis of Z-scheme $AgIn_5S_8$/Bi_2WO_6 nano-heterojunction with excellent performance for photocatalytic degradation and Cr(VI) reduction, J. Alloys Compd. 805 (2019) 41–49. https://doi.org/https://doi.org/10.1016/j.jallcom.2019.06.331.

[110] J. Dong, J. Hu, A. Liu, J. He, Q. Huang, Y. Zeng, W. Gao, Z. Yang, Y. Zhang, Y. Zhou, Z. Zou, Simple fabrication of Z-scheme $MgIn_2S_4$/Bi_2WO_6 hierarchical heterostructures for enhancing photocatalytic reduction of Cr(vi), Catal. Sci. Technol. 11 (2021) 6271–6280. https://doi.org/10.1039/D1CY01178B.

[111] Z. Wei, M. Endo, K. Wang, E. Charbit, A. Markowska-Szczupak, B. Ohtani, E. Kowalska, Noble metal-modified octahedral anatase titania particles with enhanced activity for decomposition of chemical and microbiological pollutants, Chemi. Engi. J. 318 (2017) 121–134. https://doi.org/10.1016/j.cej.2016.05.138.

[112] M. Endo, Z. Wei, K. Wang, B. Karabiyik, K. Yoshiiri, P. Rokicka, B. Ohtani, A. Markowska-Szczupak, E. Kowalska, Noble metal-modified titania with visible-light activity for the decomposition of microorganisms, Beilstein J. Nanotechnol. 9 (2018) 829–841. https://doi.org/10.3762/bjnano.9.77.

[113] A. Markowska-Szczupak, P. Rokicka, K. Wang, M. Endo, A.W. Morawski, E. Kowalska, Photocatalytic Water Disinfection under Solar Irradiation by d-Glucose-Modified Titania, Catalysts . 8 (2018). https://doi.org/10.3390/catal8080316.

[114] J. Hu, D. Chen, Z. Mo, N. Li, Q. Xu, H. Li, J. He, H. Xu, J. Lu, Z-Scheme 2D/2D Heterojunction of Black Phosphorus/Monolayer Bi_2WO_6 Nanosheets with Enhanced Photocatalytic Activities, Angew. Chem. Int. Ed. 58 (2019) 2073–2077. https://doi.org/doi:10.1002/anie.201813417.

[115] M. Zhang, J. Lu, C. Zhu, Y. Xiang, L. Xu, T. Chen, Photocatalytic degradation of gaseous benzene with Bi_2WO_6/Palygorskite composite catalyst, Solid State Sci. 90 (2019) 76–85. https://doi.org/https://doi.org/10.1016/j.solidstatesciences.2019.01.012.

[116] H. Zhou, Z. Wen, J. Liu, J. Ke, X. Duan, S. Wang, Z-scheme plasmonic Ag decorated WO_3/Bi_2WO_6 hybrids for enhanced photocatalytic abatement of chlorinated-VOCs under solar light irradiation, Appl. Catal. B. 242 (2019) 76–84. https://doi.org/https://doi.org/10.1016/j.apcatb.2018.09.090.

[117] Y. Liu, Y. Zhou, Q. Tang, Q. Li, S. Chen, Z. Sun, H. Wang, A direct Z-scheme Bi_2WO_6/NH_2-UiO-66 nanocomposite as an efficient visible-light-driven photocatalyst for NO removal, RSC Adv. 10 (2020) 1757–1768. https://doi.org/10.1039/C9RA09270F.

[118] Y. Jing, A. Fan, J. Guo, T. Shen, S. Yuan, Y. Chu, Synthesis of an ultrathin MnO_2 nanosheet-coated Bi_2WO_6 nanosheet as a heterojunction photocatalyst with enhanced photocatalytic activity, Chem. Eng. J. 429 (2022) 132193. https://doi.org/https://doi.org/10.1016/j.cej.2021.132193.

[119] W. Hu, F. Wu, W. Liu, Facile synthesis of Z-scheme Bi_2O_3/Bi_2WO_6 composite for highly effective visible-light-driven photocatalytic degradation of nitrobenzene, Chem. Phys. 552 (2022) 111377. https://doi.org/https://doi.org/10.1016/j.chemphys.2021.111377.

[120] L. Yuan, B. Weng, J.C. Colmenares, Y. Sun, Y.-J. Xu, Multichannel Charge Transfer and Mechanistic Insight in Metal Decorated 2D–2D Bi_2WO_6–TiO_2 Cascade with Enhanced Photocatalytic Performance, Small. 13 (2017) 1702253. https://doi.org/doi:10.1002/smll.201702253.

[121] A.R. Mahammed Shaheer, N. Thangavel, R. Rajan, D.A. Abraham, R. Vinoth, K.R. Sunaja Devi, M. V Shankar, B. Neppolian, Sonochemical assisted impregnation of Bi_2WO_6 on TiO_2 nanorod to form Z-scheme heterojunction for enhanced photocatalytic H_2 production, Adv Powder Technol. 32 (2021) 4734–4743. https://doi.org/https://doi.org/10.1016/j.apt.2021.10.022.

[122] L. Yuan, K.-Q. Lu, F. Zhang, X. Fu, Y.-J. Xu, Unveiling the interplay between light-driven CO_2 photocatalytic reduction and carbonaceous residues decomposition: A case study of Bi_2WO_6-TiO_2 binanosheets, Appl. Catal. B. 237 (2018) 424–431. https://doi.org/https://doi.org/10.1016/j.apcatb.2018.06.019.

[123] H. Hori, M. Takashima, M. Takase, B. Ohtani, Pristine Bismuth-tungstate Photocatalyst Particles Driving Organics Decomposition through Multielectron Reduction of Oxygen, Chem. Lett. 46 (2017) 1376–1378. https://doi.org/10.1246/cl.170570.

[124] H. Hori, M. Takashima, M. Takase, M. Kitamura, F. Amano, B. Ohtani, Multielectron reduction of molecular oxygen in photocatalytic decomposition of organic compounds by bismuth tungstate particles without cocatalyst loading, Catal. Today. 303 (2018) 341–349. https://doi.org/https://doi.org/10.1016/j.cattod.2017.08.045.

[125] H. Hori, M. Takashima, M. Takase, B. Ohtani, Kinetic analysis supporting multielectron reduction of oxygen in bismuth tungstate-photocatalyzed oxidation of organic compounds, Catal. Today. 313 (2018) 218–223. https://doi.org/https://doi.org/10.1016/j.cattod.2018.01.001.